IgM Natural Antibodies Bind HLA-E-Leader Peptide Complexes and Modulate NK Cell Cytotoxicity

Dapeng Li[1,#], Simon Brackenridge[4,#], Lucy C. Walters[4,#], Karl Harlos[5], Daniel Rozbesky[5,6], Derek W. Cain[1,2], Kevin Wiehe[1,2], Richard M. Scearce[1], Maggie Barr[1], Zekun Mu[1], Robert Parks[1], Max Quastel[4], Robert J. Edwards[1,2], S. Munir Alam[1,2], Kevin O. Saunders[1,4], Persephone Borrow[4], E. Yvonne Jones[5], Geraldine M. Gillespie[4,*], Andrew J. McMichael[4,*], Barton F. Haynes[1,3,*]

[1]Duke Human Vaccine Institute, Duke University School of Medicine, Durham, NC 27710, USA

[2]Department of Medicine, Duke University School of Medicine, Durham, NC 27710, USA

[3]Department of Immunology, Duke University School of Medicine, Durham, NC 27710, USA

[4]Nuffield Department of Clinical Medicine, University of Oxford, Oxford, OX3 7FZ, UK

[5]Division of Structural Biology, Wellcome Centre for Human Genetics, University of Oxford, Oxford, OX3 7BN, UK

[6]Department of Cell Biology, Charles University, Prague, 12800, Czech Republic

[#]Authors contributed equally

*Address correspondence to geraldine.gillespie@ndm.ox.ac.uk, andrew.mcmichael@ndm.ox.ac.uk and barton.haynes@duke.edu

ABSTRACT (147 words)

The non-classical class Ib molecule human leukocyte antigen E (HLA-E) has limited polymorphism and can bind HLA class Ia leader sequence peptides (VL9). HLA-E-VL9 complexes interact with the natural killer (NK) cell inhibitory receptor NKG2A/CD94 and regulate NK cell-mediated cytotoxicity. Here we report a murine HLA-E-VL9-specific IgM monoclonal antibody 3H4 that enhanced killing of HLA-E-VL9-expressing target cells by a $NKG2A^+$ NK cell line, most likely due to steric clashes between 3H4 and CD94/NKG2A when docked on the HLA-E-VL9 surface as determined by a 1.8 Å co-complex crystal structure. Key 3H4-mediated contacts with HLA-E-VL9 were generated by germline-encoded CDR-H3 residues. Human IgM HLA-E-VL9 reactive antibodies could also be isolated from $CD10^-/CD27^-$ naïve B cells; these antibodies also recognized microbiome-derived peptides presented by HLA-E. Thus, a subset of natural antibodies that recognize VL9-bound HLA-E exist as part of the normal Ig repertoire with capacity to regulate NK cell function.

INTRODUCTION

Natural killer (NK) cells play critical roles in immune surveillance by discriminating non-self from self, and function as effector cells by killing non-self malignant or pathogen-infected cells and producing inflammatory cytokines (Chiossone et al., 2018; Raulet, 2006; Yokoyama and Kim, 2006). Specific recognition of non-self by NK cells relies on a series of activating and inhibitory receptors, including the killer immunoglobulin-like receptor (KIR) family and the NKG2/CD94 heterodimeric receptors (Andre et al., 2018; Chiossone et al., 2018). NK cell inhibitory receptors ligate human lymphocyte antigen (HLA) or major histocompatibility complex (MHC) class I molecules expressed on healthy cells as self. Conversely, cells lacking MHC class I are recognized by NK cells as “missing-self” and are sensitive to NK cell-mediated killing (Ljunggren and Karre, 1985, 1990). In humans, KIRs recognize classical human HLA class Ia molecules (Colonna and Samaridis, 1995; Karlhofer et al., 1992; Pende et al., 2019), whereas the inhibitory NKG2A/CD94 heterodimeric receptor interacts with the non-classical HLA class Ib molecule HLA-E and is balanced by an activating receptor NKG2C/CD94 (Braud et al., 1997; Braud et al., 1998; Brooks et al., 1997). While KIRs expression is heterogeneous,, NKG2A/CD94 is expressed on ~40% of human NK cells (Andre et al., 1999; Mahapatra et al., 2017; Pende et al., 2019). Similarly, unlike classical HLA class I molecules, HLA-E has limited polymorphism with only two predominant expressed variants HLA-E*01:01 and HLA-E*01:03 that differ only in residue 107, which is outside the peptide-binding groove (Kraemer et al., 2014). The NKG2A/CD94/HLA-E pathway is considered as an important immune checkpoint target and has recently become a focus for NK cell-based immunotherapeutic strategies (Hu et al., 2019; Kim et al., 2019; Souza-Fonseca-Guimaraes et al., 2019). A subset of CD8+ T cells also express NKG2A/CD94, and inhibition of NKG2A/CD94 - HLA-E interaction similarly has application in CD8+ T cell-based immunotherapy (Andre et al., 2018; van Montfoort et al., 2018).

HLA-E engages with NKG2A/CD94 via a restricted subset of peptides VMAPRT(L/V)(V/L/I/F)L (designated VL9) that derive from the leader sequence of HLA-A, -C, -G and a third of HLA-B molecules (Braud et al., 1997; Braud et al., 1998; Lee et al., 1998a; Lee et al., 1998b). HLA-E binds VL9 peptides, which stabilize HLA-E surface expression (Braud et al., 1997; Braud et al., 1998) on healthy host cells in which HLA-Ia expression is not perturbed and initiate recognition by NKG2A/CD94 or NKG2C/CD94 on NK cells. The binding affinity of HLA-E-VL9 peptide complexes for NKG2A/CD94 is greater than that for NKG2C/CD94, such that the inhibitory signal dominates to suppress aberrant NK cell-mediated cytotoxicity as well as cytokine production (Aldrich et al., 1994; Braud et al., 1998; Kaiser et al., 2008; Llano et al., 1998; Rolle et al., 2018). In addition, HLA-E and its murine or rhesus macaque homologs, is capable of binding to a range of other host peptides and pathogen-derived peptides, including heat-shock protein 60 (Hsp60)-derived peptides (Michaelsson et al., 2002), Mycobacterium tuberculosis (Mtb) peptides (Joosten et al., 2010; van Meijgaarden et al., 2015), and simian immunodeficiency virus (SIV) Gag peptides (Hansen et al., 2016), though unusually with a lower affinity than VL9 (Walters et al., 2020). However, only VL9 peptide-loaded HLA-E can engage CD94/NKG2A and protect cells from NK cell cytotoxicity (Kraemer et al., 2015; Michaelsson et al., 2002; Sensi et al., 2009). Hence, leader sequence VL9 peptides are essential not only for stabilizing HLA-E surface expression but also for determining the role of HLA-E/NKG2A/CD94 pathway in regulating NK cell self-recognition. However, it remains unclear if interruption of this pathway by specifically targeting HLA-E-peptide complexes can enhance NK cell activity.

Natural antibodies are immunoglobulins that are present prior to simulation by cognate antigen, and provide the first line of defence against bacterial, fungal and viral infections (Holodick et al., 2017). They also suppress autoimmune, inflammatory and allergic responses, protect from atherosclerotic vascular injury, and mediate apoptotic cell clearance (New et al., 2016). Natural antibodies are generally near germline in sequence, have repertoire skewing of

IgM, IgA or IgE isotype, and respond to antigens with T cell independence (Holodick et al., 2017). However, specific roles in regulation of natural killer (NK) cell functions are unknown.

Here, we define a mechanism of natural antibody modulation of NK cell killing whereby a murine IgM monoclonal antibody (mAb) 3H4 bound to HLA-E-VL9 on target cells and enhanced NK cytotoxicity of a NKG2A+ NK cell line. X-ray crystallographic analysis of an HLA-E-VL9/3H4 antigen-binding fragment (Fab) co-complex indicated that due to steric clashes, 3H4 and CD94/NKG2A cannot simultaneously bind to what are essentially overlapping recognition surfaces on HLA-E-VL9. Key Ig V(D)J residues in the 3H4-HLA-E-VL9 binding interface were germline-encoded. Similarly, human HLA-E-VL9-reactive, near-germline IgMs were isolated from the naïve B cell repertoire that recognized microbiome VL9-like peptides presented by HLA-E. Thus, a subset of natural IgM HLA-E-VL9 antibodies exist *in vivo* that have the potential to regulate NK cell cytotoxicity.

RESULTS

Isolation of an HLA-E-VL9-specific mAb 3H4 from immunized transgenic mice

With the original intention of raising monoclonal antibodies to the HIV-1 Gag peptide RMYSPTSIL (RL9HIV) (the HIV counterpart of RL9SIV, one of the MHC-E binding SIV Gag peptides identified by Hansen et al., 2016), we immunized human HLA-B27/β2-microglobulin (β2M) transgenic mice (Taurog et al., 1990) (***Figures S1A-B***) with 293T cells transfected with surface-expressed single chain HLA-E-RL9HIV complexes (Yu et al., 2002) (***Figure 1A*** and ***S1C-D***). We produced hybridomas, and culture supernatants were screened for binding on a panel of 293T cells transfected with single chain HLA-E-RL9HIV peptide complexes, or with single chain HLA-E-VL9 peptide complexes as a control. Unexpectedly, we isolated a subset of antibodies that specifically reacted with HLA-E-VL9 peptide, the most potent of which was the IgM mAb 3H4. Unlike the well-characterized pan-HLA-E mAb 3D12 (Marin et al., 2003), 3H4 reacted specifically with HLA-E-VL9 (VMAPRTLVL) and not with control, non-VL9 HLA-E-

peptide complexes (***Figure 1B***). Mab 3H4 also bound to VL9 peptide-pulsed HLA-class I negative K562 cells transfected with HLA-E (Lampen et al., 2013) (***Figure 1C***). Moreover, 3H4 bound to soluble HLA-E refolded with synthetic VL9 peptide in both ELISA (***Figure 1D***) and surface plasmon resonance (SPR) assays (***Figure 1E***).

HLA-E-VL9-specific mAb 3H4 is a minimally mutated pentameric IgM

Sequence analysis of 3H4 mAb revealed 1.04% heavy chain variable region (V_H) and 2.51% light chain viable region (V_L) mutations *(**Table S1**)*. We isolated 3 additional mAbs from another two immunization studies (see methods). All four HLA-E-VL9-specific mouse antibodies isolated were minimally mutated IgM (mean VH and VL mutations, 1.21% and 2.87%, respectively) (***Table S1***). Negative stain electron microscopy showed that 3H4 was predominantly pentameric with a small proportion of hexamers (***Figures S2A-B***). In addition, 3H4 was not autoreactive in anti-nuclear antibody or clinical autoantibody tests (***Figures S3A-B***).

3H4 IgM enhances NK cell cytotoxicity against HLA-E-VL9-expressing target cells

Given the suppressive role of the HLA-E-VL9/NKG2A/CD94 pathway in NK cell function, we tested whether the binding of mAb 3H4 to HLA-E-VL9 could block NKG2A/CD94 interaction with HLA-E and thereby release NK cell function (***Figure 2A***). A NKG2A/CD94 expressing human NK cell line, NK92 (***Figure S4***), exhibited increased cytotoxicity against HLA-E-VL9 overexpressing cells in the presence of 3H4 IgM compared to an isotype control IgM (***Figure 2B***). Next, we engineered the 3H4 variable regions into a human IgG2σ backbone (Saunders, 2019) (***Figure S5***). The 3H4-human IgG retained binding specificity for HLA-E-VL9, but showed no cytotoxicity enhancement of NK cells (***Figure 2C***). In addition, we tested a combination of 3H4 with the NKG2A specific antibody, Z199. While blocking NKG2A enhanced NK killing against HLA-E-VL9 expressing cells (***Figure 2D***), no further elevated killing was observed when

combining 3H4 with Z199 (***Figure 2E***), suggesting that killing enhancement was maximal with 3H4 alone. These data demonstrated that HLA-E-VL9-specific mAb 3H4 could enhance the killing capacity of NKG2A+ NK cells, and this immunoregulatory role of 3H4 was dependent on its IgM pentameric form, probably due to higher avidity binding.

3H4 IgM recognizes the α1/α2 domain of HLA-E and N-terminus of the VL9 peptide

To map the epitope on the HLA-E-VL9 complex recognized by 3H4, we tested 3H4 binding to VL9 peptide presented by HLA-E, the rhesus ortholog Mamu-E, as well as two HLA-E/Mamu-E hybrids – one with HLA-E α1/Mamu-E α2 (Hα1/Mα2), the other with Mamu-E α1/HLA-E α2 (Mα1/Hα2). 3H4 did not bind to Mamu-E/VL9 nor Hα1/Mα2-VL9, and its staining of cells expressing Mα1/Hα2-VL9 was weak (***Figure 3A***), suggesting that 3H4 recognition involves interaction with both α1 and α2 domains of HLA-E, and the epitope on α2 might be partially conserved between human and rhesus. Moreover, VL9 mutation indicated that position 1 (P1) of the peptide is important for 3H4 binding (***Figure 3B***), with antibody recognition of VL9 peptide P1 variants with alanine, cysteine, isoleucine, serine, threonine, weak binding to histidine and proline, but not those with arginine, glutamate, glycine, lysine, methionine, asparagine, tryptophan, tyrosine or phenylalanine (***Figures 3C and S6***). These data suggest that mAb 3H4 makes contacts with both the HLA-E α1/α2 domain and the amino-terminal end of the VL9 peptide.

Co-complex crystal structure of a 3H4 Fab bound to HLA-E-VL9

We obtained a co-complex crystal structure of the 3H4 Fab bound to VL9 peptide-loaded HLA-E, which packed in the C2 space group and diffracted to 1.8 Å (***Table S2***). Although two copies of the co-complex were present in the asymmetric unit, a single copy constitutes the focus of further discussion here since root-mean-square deviation (RMSD) calculations from Cα-atom pairwise alignment of the two copies indicated minimal repositioning of interfacing

residues at the HLA-E-3H4 binding site (***Table S3***). Additionally, pairwise alignment with the previously published non-receptor-bound HLA-E coordinates (PDB: 1MHE) (O'Callaghan et al., 1998) revealed minimal structural changes in HLA-E upon 3H4 engagement (***Table S3B***).

3H4 docked onto the N-terminal region of the HLA-E-peptide-binding groove making contacts with both α-helices of the HLA-E heavy chain in addition to residues 1-4 of the VL9 peptide (***Figures 4A-B***). The 3H4-HLA-E interface was mainly mediated via electrostatic interactions and was dominated by the 3H4 VH chain segment which created a total buried surface area of 1109.4 $Å^2$ and formed ten hydrogen bonds (H-bonds) and three salt bridges with HLA-E residues of the α1-helix and one H-bond with T163 of the HLA-E α2-helix. By contrast, the smaller 3H4 VL chain-HLA-E interface buried 522.8 $Å^2$ and involved only three inter-molecular H-bonds and three salt bridges (***Tables S3 and S4***). Superposition of the 3H4-HLA-E-VL9 co-complex with a previously published HLA-E-bound CD94/NKG2A structure (Kaiser et al., 2008; Petrie et al., 2008) revealed steric clashes between the VH and VL domains of 3H4 and the CD94 and NKG2A subdomains, respectively (***Figures 4C-D***). Moreover, seven HLA-E heavy chain residues (positions 58, 59, 62, 63 on the α1 helix and 162, 163 and 167 on the α2 helix) are shared between the 3H4-HLA-E and CD94/NKG2A-HLA-E footprints (***Figures 4E-F***). Such steric clashes and overlapping footprints suggest simultaneous docking of these two HLA-E binding partners, 3H4 and NKG2A/CD94, would be disallowed.

Germline-encoded residues are critical for 3H4 contact with both HLA-E and VL9 peptide

Remarkably, all four of the 3H4-derived residues that interface with the VL9 peptide (Y97, S100, S100A and Y100B, Kabat numbering) reside within the VH CDR3 D-junction and are germline-encoded. This 3H4-VL9 interface is characterized by weak Van der Waals and hydrophobic contacts, such as those mediated between Y100B (3H4) and V1 or P4 (VL9) (***Figure 4G***). Further, the positioning of the Y100B (3H4) side chain directly above V1 (VL9) in part explains the preference for small side chains at this position of the peptide and the dramatic

reductions in 3H4 binding to HLA-E bound to VL9 variants with larger residues such as H or F at position 1 (***Figure 3C***). Distinctive shape complementarity is also observed at the 3H4-VL9 interface with the side chains of S100 and S100A (3H4) wrapping around the cyclic side chain of P4 (VL9).

The germline-encoded VH CDR3 D-junction residues that form the 3H4-VL9 interface (Y97, S100, S100A and Y100B), also mediate key contacts with the HLA-E heavy chain. The surface loop (residues A93-V102) containing these germline-encoded residues sweeps across the HLA-E-peptide-binding groove forming H-bonds with both the α1 and α2 helices; T163 of the HLA-E α2 helix forms a H-bond with S100 (3H4), and R62 of the HLA-E α1-helix forms two H-bonds with the Y100B (3H4) mainchain and an additional H-bond with the main chain of S100A (3H4) (***Figure 4H***). Moreover, Y100B (3H4) is involved in multiple polar pi stacking interactions. Not only is the Y100B side chain sandwiched between R62 and W167 of the HLA-E α1 and α2 helices, respectively, R62 (HLA-E α1) is also positioned between the aromatic rings of Y100B and W100D of the VH CDR3 domain.

Key contacts outside the germline-encoded CDR3 D-junction region are also formed at the 3H4 VH-HLA-E or 3H4 VL-HLA-E interfaces. For 3H4 HC, the VH CDR2 region (residues I51-T57) is positioned above the HLA-E α1-helix where a string of inter-molecular H-bonds are formed involving G56 and N54 of the VH CDR2 in addition to D50, Q61 and K64 of the framework VH chain region (***Figure 4H***). Critically, R65 of the HLA-E α1-helix forms four H-bonds with the 3H4 VH and also mediates polar pi stacking interactions with W100D of the VH CDR3 loop. For 3H4 LC, D92 and E93 of the VL CDR3 loop H-bond with K170 of the HLA-E α2-helix and N30 of the VL CDR1 loop forms an H-bond with the α2-helix residue, E166, of HLA-E (***Figure 4I***). It is noteworthy that the four key interfacing residues of the 3H4 VH CDR3 D-junction (Y97, S100, S100A and Y100B) are germline-encoded (***Figures 4J***). Since these residues interface with both the HLA-E heavy chain and VL9 peptide, the B cell receptor

germline component plays a central role in the recognition of VL9-bound HLA-E complexes by 3H4.

Germline-encoding HLA-E-VL9-specific antibodies exist in healthy humans

That HLA-E-VL9-specific antibodies were isolated from mice immunized with an unrelated peptide antigen (RL9HIV) implied that antibody 3H4 might be derived from the natural B cell pool rather than induced by immunization. Therefore, we assessed binding of HLA-E-VL9 fluorescent tetramers to B cells from naïve HLA-B27/β2M TG mice and B6 mice, and found that HLA-E-VL9-binding B cells existed in unimmunized mice (***Figure S7***). Additionally, all HLA-E-VL9-specific antibodies were minimally mutated IgM antibodies (***Table S1***). These findings raised the hypothesis that HLA-E-VL9-specific antibodies were natural antibodies in mice.

We next questioned if similar antibodies were present in humans. Using HLA-E-VL9 tetramers as probes, we identified B cells expressing HLA-E-VL9-specific B cell receptors (BCRs) in four male, cytomegalovirus (CMV) seronegative human donors (***Figures 5A and S8, Table S5***). We isolated 56 HLA-E-VL9-specific antibodies (***Figure 5B, Table S6***) that specifically reacted with HLA-E-VL9 complexes (***Figures S9-S10***). By performing more in-depth analysis of the binding profiles of four representative antibodies - CA123, CA133, CA143 and CA147, we found that these antibodies exhibited distinct binding specificities to VL9 peptide variants (***Figure 5C***) in addition to differential cross-reactivities with rhesus Mamu-E-VL9 or mouse Qa-1-VL9 complexes (***Figure S11A-D***). These data suggested that BCRs with diverse recognition patterns on the HLA-E-VL9 complex are present in uninfected humans.

In different donors, the percentages of HLA-E-VL9-specific B cells in pan-B cells ($CD3^-CD235^-CD14^-CD16^-CD19^+$) was 0.0009%-0.0023% (mean of 0.0014%) (***Figure 5D***). HLA-E-VL9-specific B cells were $IgD^+IgM^{+/-}$ B cells, in which four cell subsets were observed (***Figure 5E***) – $CD10^-CD27^-CD38^{+/-}$ naïve B cells (71.4%), $CD10^+CD27^-CD38^{++}$ immature or newly formed B cells (Giltiay et al., 2019) (10.7%), and $CD10^-CD27^+CD38^-$ non-class-switched

memory cells, demonstrating that BCRs specifically targeting HLA-E-VL9 peptide existed in the naïve B cell repertoire of healthy humans.

V_H/V_L gene usage of HLA-E-VL9-specific antibodies

Natural antibodies demonstrate Ig repertoire skewing (Holodick et al., 2017; New et al., 2016). To characterize the human antibody gene usage of HLA-E-VL9 antibodies, we analyzed the paired heavy chain and light chain gene sequences of 56 human HLA-E-VL9 antibodies, and found 1 multiple-member clone containing 6 antibodies in donor LP021 (Kepler et al., 2014) (***Table S7***). Next, we compared the 51 HLA-E-VL9-specific B cell clones with a reference human antibody repertoire (DeKosky et al., 2015). Over 45% of the heavy chain variable region (V_H) genes were VH3-21 or VH3-11 in HLA-E-VL9 antibodies, whereas less than 7% of the control B cells used these two genes (***Figure 6A*** *and* ***Table S6***). HLA-E-VL9 antibodies light chain variable region (V_κ/V_λ) also preferentially utilized IGKV3-15, IGKV1-39 and IGKV3-11 genes compared to controls (***Figure 6B*** *and* ***Table S6***). No J chain gene usage preference was observed (***Figure S12***). Moreover, HLA-E-VL9 antibodies showed a trend to have shorter heavy chain complementarity determining region 3 (CDR3) lengths than the reference antibodies (***Figure 6C***), while no difference was observed for light chain CDR3 (***Figure 6D***). Given HLA-E-VL9 antibodies were all IgMs primarily from naïve or immature B cells, we compared the mutation frequencies of 51 clones with a reference human antibody repertoire containing both naïve and antigen-experienced antibodies (DeKosky et al., 2016). Both heavy and light chain variable region genes exhibited low somatic mutation rates that were similar to naïve B cell controls (***Figures 6E-F***). Thus, human HLA-E-VL9-specific antibodies were IgM, minimally mutated and displayed skewed usage of VH3-21 and VH3-11 VHs and IGKV3-15, IGKV1-39 and IGKV3-11 VLs.

HLA-E-VL9-specific mAbs recognize microbiome-derived VL9-like peptides presented by HLA-E

We identified microbiome-derived VL9-like peptides from the NCBI microbiome database predicted by NetMHC to have HLA-E binding capacity (Andreatta and Nielsen, 2016; Nielsen et al., 2003) (***Table S7***). Eight peptides with the highest HLA-E binding scores were synthesized as 9 amino acid peptides, incubated with K562-E cells, and tested for mAb 3H4 HLA-E-VL9-specific antibody binding. Seven out of eight microbiome sequence-derived peptides showed strong HLA-E binding as indicated by the ability to stabilize and upregulate HLA-E expression, as read out by staining with HLA-E reactive antibody, 3D12 (***Figures 7 and S13A***). Notably, peptides with sequences very closely related to VL9 (VMAPRTLLL), VMPPRALLL (from *Escherichia coli MS 175-1*), VMAGRTLLL (from *Stenotrophomonas sp.*) and VMAPRTKLL (from *Pseudomonas formosensis*) were detected on K562-E cells by the HLA-E-peptide-antibody 3H4. Human HLA-E-VL9 antibodies CA143 and CA147 also reacted with *Pseudomonas formosensis*-derived peptide VMAPRTKLL bound to HLA-E (Lin et al., 2013) (***Figures 7 and S13B-C***). These data demonstrate that microbiome-derived peptides in complex with HLA-E are capable of binding to HLA-E-VL9-specific antibodies and raise the hypothesis that microbiome peptides may be one type of antigen capable of stimulating B cells with HLA-E-VL9 peptide specificity *in vivo.*

DISCUSSION

In this study, we have isolated and characterized antibodies reactive with HLA-E-VL9 peptide complexes, and found these antibodies were derived from the naïve IgM B cell BCR repertoire in mice as well as in non-immunized, HCMV seronegative male humans. While more than 80% of the HLA-E-VL9 reactive B cells were immature or naïve, a few showed a memory or plasmablast phenotype. However, somatic mutations were minimal and the affinity was low. The lack of class switching in HLA-E-VL9-specific antibodies may reflect self-tolerance of CD4 T

cells and a lack of help for maturation of these antibodies. While the mouse antibodies were selected in the setting of HLA-E-unrelated peptide immunizations, they were minimally mutated IgM antibodies, as were most of the antibodies isolated from un-infected human males. Structural analysis of the HLA-E-VL9:3H4 Fab co-complex revealed that the 3H4 heavy chain made key contacts with HLA-E and the VL9 peptide using germline-encoded residues in the CDR-H3 (D) region (***Figure 4J***). However, 3H4 is a mouse antibody reacting with human HLA-E-VL9. The HLA-E equivalent in C57BL/6xSJL mice is Qa1b which presents the very similar class Ia signal peptide 'Qdm' AMAPRTLLL. Whilst 3H4 recognizes that peptide bound to HLA-E, it does not bind to that peptide in Qa1b (***Figure S6B***). However, HLA-E-VL9-specific antibodies were identified in the naïve B cell pool of healthy humans, so the question arises as to whether such B cells, or the antibodies they can produce, play an important immunoregulatory role in humans. If so, this might provide the selective force to maintain these enriched V genes in the germline. Indeed, we demonstrated proof of concept that the 3H4 IgM HLA-E-VL9 antibody could enhance NK cytotoxicity of NKG2A+ NK cells.

Autoantibodies to HLA-Ia (Alberu et al., 2007; Morales-Buenrostro et al., 2008) and HLA-E heavy chains (Ravindranath et al., 2010a; Ravindranath et al., 2010b) have been detected in non-alloimmunized males, and contribute to allograft damage (Hickey et al., 2016; McKenna et al., 2000). It has been suggested that the HLA-E antibodies in non-alloimmunized humans could be elicited by autoantigens derived from viral, bacterial, or environmental agents cross-reactive with HLAs, or soluble HLA-E heavy chains that become immunogenic without the β2M subunit (Alberu et al., 2007; Hickey et al., 2016; Ravindranath et al., 2010a; Ravindranath et al., 2010b). Viruses, bacteria and other microbes could be the stimuli of such innate-adaptive immune interaction. The best known example is human cytomegalovirus (HCMV) that encodes the VL9 sequence VMAPRTLIL in the leader sequence of its UL40 gene. This peptide is processed in a TAP independent manner and presented bound to HLA-E at the cell surface to inhibit NK cell killing and evade innate immune responses (Tomasec et al., 2000). This has not been reported

316 to elicit antibody responses, but HLA-E-UL40 peptide-specific T cells have been described
317 when the limited polymorphism in the HLA A, B and C sequences mismatches that of the virus
318 to overcome self-tolerance (Sullivan et al., 2015). However, these subjects in this study were all
319 HCMV seronegative, ruling out the possibility that these antibodies were HCMV-induced.
320 Similarly, that they were male excluded pregnancy induced priming. A recent study found that
321 mouse gut microbial antigens shaped the BCR repertoire by contributing to BCR selection and
322 affinity maturation (Chen et al., 2020). Therefore, we tested several potential HLA-E binding
323 peptides, with sequence similarities to VL9, derived from the human microbiome. Three of our
324 HLA-E-VL9 antibodies recognized a subset of these HLA-E-presented microbiome-derived VL9-
325 like peptides. These data imply that human microbial peptides could also be presented by HLA-
326 E, interact with HLA-E-VL9-bound naïve BCRs, and trigger expansion of B cells that express
327 HLA-E-VL9-specific BCRs.

328 Harnessing NK cells to attack tumor cells has emerged as an attractive strategy for cancer
329 immunotherapies (Guillerey et al., 2016; Lowry and Zehring, 2017). One of the most promising
330 targets for therapeutic immune-modulation of NK cell functions is the NKG2A/CD94-HLA-E-VL9
331 interaction. Monalizumab, the first-in-class monoclonal antibody checkpoint inhibitor targeting
332 NKG2A, enhances anti-tumor immunity by activating cytotoxic activities of effector CD8+ T cells
333 and NK cells (Andre et al., 2018; Creelan and Antonia, 2019; van Hall et al., 2019). In our study,
334 co-complex structural analysis revealed steric clashes between a 3H4 Fab and the NK inhibitory
335 receptor NKG2A/CD94 when docked onto HLA-E-VL9, which explained the mechanism of 3H4
336 IgM enhancing NKG2A+ NK cell killing. Notably, 3H4 IgM enhanced the cytotoxicity of an
337 NKG2A+ human NK cell line NK92, that is a safe and established cell line for adoptive
338 immunotherapy in phase I clinical trials (Klingemann et al., 2016). Therefore, 3H4 which targets
339 HLA-E-VL9 could have potential as an alternative to NKG2A targeting antibodies such as
340 Monalizumab as a check point inhibitor for immunotherapy.

In summary, our study has demonstrated a novel specificity of IgM natural antibodies, that of recognition of HLA-E-VL9 peptide complexes, which suggests a NK cell immunoregulatory role. The isolation of antibody 3H4 suggested that mouse could be a repository for this and other anti-HLA-E-peptide antibodies that warrant further development as therapeutic agents. Finally, the methods used here provide a means to rapidly isolate mAbs to other HLA/peptide complexes such as HLA-E-SIV/HIV peptides (Hansen et al., 2016; Walters et al., 2018), mycobacterium tuberculosis peptides (Joosten et al., 2010; McMurtrey et al., 2017; van Meijgaarden et al., 2015), or HLA class I-presented neoantigen peptides that are derived from mutated tumor tissues (Chen et al., 2019; Garcia-Garijo et al., 2019).

MATERIALS AND METHODS

Cell Lines

K562-E cells (K562 cells stably expressing HLA-E) and K562-E/UL49.5 cells (with a TAP-inhibitor UL49.5) are kindly provided by Dr. Thorbald van Hall from Leiden University (Lampen et al., 2013). All the other cells used in this study are from ATCC. 293T cells (ATCC CRL-3216) were maintained in Dulbecco's Modified Eagle's Medium (DMEM; Gibco, Catalog# 10564) supplemented with 10% fetal bovine serum (FBS; Gibco, Catalog# 10099141) and 1% penicillin/streptomycin (Gibco, Catalog# 10378016). K562 cells (ATCC CCL-243), K562-E cells and K562-E/UL49.5 cells were cultured in Iscove's Modified Dulbecco's Medium (IMDM; Hyclone, Catalog# SH30228.01) supplemented with 10% FBS. Jurkat, DU-4475 and U-937 cells were cultured in RPMI-1640 medium (Gibco, Catalog# 72400) supplemented with 10% FBS. SiHa cells were cultured in Minimum Essential Medium (MEM; Gibco, Catalog# 11095080) supplemented with 10% FBS. The NK-92 human cell line (ATCC CRL-2407) was cultured in Alpha Minimum Essential medium (α-MEM; Gibco, Catalog# 12561072) supplemented with 2 mM L-glutamine, 0.2 mM inositol, 0.1 mM 2-mercaptoethanol, 0.02 mM folic acid, 100 U/ml

recombinant IL-2 (Biolegend, Catalog# 589108), 12.5% horse serum (Gibco, Catalog# 16050122) and 12.5% FBS. All the cells were maintained at 37°C, 5% CO2 in humidified incubators.

Animals

Transgenic mice carrying human β2-microglobulin (β2m) and HLA-B*27:05 genes were obtained from Jackson lab (B6.Cg-Tg(B2M,HLA-B*27:05)56-3Trg/DcrJ; Stock# 003428). Hemizygous mice were used in this experiment, as this strain is homozygous lethal. For hemizygous mice genotyping, peripheral blood lymphocytes (PBLs) were isolated and stained using mouse CD45 antibody (Biolegend, Catalog# 103122), human HLA class I antibody (Biolegend, Catalog# 311406) and human β2m antibody (Biolegend, Catalog# 316312). All animal experiments were conducted with approved protocols from the Duke University Institutional Animal Care and Use Committee.

Human Subjects

Human leukapheresis frozen vials were collected by the External Quality Assurance Program Oversight Laboratory (EQAPOL) (Sanchez et al., 2014a; Sanchez et al., 2014b). Samples from four male donors were used in this study. ***Table S5*** shows the clinical characteristics of the individuals studied. All experiments that related to human subjects was carried out with the informed consent of trial participants and in compliance with Institutional Review Board protocols approved by Duke University Medical Center.

Peptide synthesis

The VL9 peptide (VMAPRTVLL) was synthesized to >85% purity via Fmoc (9-fluorenylmethoxy carbonyl) chemistry by Genscript USA and reconstituted to 200mM in DMSO.

HLA-E-peptide protein refolding and purification

β2-microglobulin, previously purified from inclusion bodies in a Urea-MES buffer, was added to a refolding buffer to achieve a final concentration of 2μM. The refold buffer comprised 100 mM Tris pH8.0, 400mM L-arginine monohydrochloride, 2mM EDTA, 5mM reduced glutathione and 0.5mM oxidized Glutathione and was prepared in MiliQ water. A 20μM concentration of VL9 peptide (VMAPRTVLL), previously reconstituted to 200mM in DMSO, was added to the refolding buffer followed by HLA-E*0103 heavy chain, which was pulsed into the refold to a final concentration of 1μM. Once the refold had incubated for 72hrs at 4 °C it was filtered through a 1.0μm cellular nitrate membrane and concentrated in the VivaFlow 50R and VivaSpin Turbo Ultrafiltration centrifugal systems with 10kDa molecular weight cut-offs. The concentrated samples were injected onto a Superdex S75 16/60 column and refolded protein eluted according to size into phosphate buffered saline (PBS). Eluted protein complexes were validated by non-reducing SDS-PAGE electrophoresis on NuPAGE 12% Bis-Tris protein gels and further concentrated via VivaSpin Turbo Ultrafiltration centrifugal device to 1.1mg/mL.

HLA-E-peptide biotinylation and tetramer generation

HLA-E-peptide samples requiring biotinylation were subsequently buffered exchanged on Sephadex G-25 PD10 columns (GE Healthcare, UK) into 10mM Tris buffer using commercially available BirA enzyme (Avidity, USA) following the manufacturer's instructions. Following overnight biotinylation, protein samples were subsequently purified into 20mM Tris pH8,100mM NaCl buffer or PBS on a HiLoad 16/600 Superdex 75pg column using an AKTA size exclusion fast protein liquid chromatography (FPLC) system. Correctly folded β2m-HLA-E*01:03-peptide complexes were subsequently concentrated to 2mg/mL and snap frozen.

HLA-E*01:03 tetramers were generated via conjugation to various fluorescent labels including Extravidin-PE (Sigma), Streptavidin-bound APC (Biolegend, San Diego) or BV421 (Biolegend, San Diego) at a Molar ratio of 4:1 as previously described (Braud et al., 1998).

419

420 **Immunization in HLA-B27/β2m Transgenic Mice**

421 HLA-B27/β2m transgenic mice (*n*=23) were intramuscularly (i.m.) immunized with pooled
422 HLA-E-RL9HIV complex (12.5 μg/animal) and HLA-E-RL9SIV complex (12.5 μg/animal)
423 adjuvanted with STR8S-C at weeks 0, 2, 4, 6, 12 and 16. MAb 3H4 was isolated from one of the
424 mice in this study. In another experiment, HLA-B27/β2m transgenic mice (*n* = 10) were i.p.
425 immunized with either HLA-E-RL9HIV SCT transfected 293T cells ($2x10^6$ cells/animal) or HLA-
426 E-RL9SIV SCT transfected 293T cells ($2x10^6$ cells/animal) at weeks 0, 2, 4, 6, 17 and 19. In the
427 third experiment, HLA-B27/β2m transgenic mice (*n*=10) were i.m. immunized with HLA-E-VL9
428 complex (25 μg/animal) adjuvanted with STR8S-C at Week 0, 2 and 4, following by
429 intraperitoneally (i.p.) immunization with HLA-E-VL9 SCT transfected 293T cells ($2x10^6$
430 cells/animal) at Week 14, 16 and 18. Serum titers were monitored by ELISA Mice with high
431 binding antibody titers were selected for the subsequent spleen cell fusion and B cell sorting
432 experiments.

433

434 **Hybridoma Cell Line Generation and Monoclonal Antibody Production**

435 Mice were boosted with the indicated priming antigen 3 days prior to fusion. Spleen cells
436 were harvested and fused with NS0 murine myeloma cells using PEG1500 to generate
437 hybridomas. After 2 weeks, supernatant of hybridoma clones were collected and screened by
438 flow cytometry-based high throughput screening (HTS). Specifically, we tested for antibodies
439 differentially binding 293T cells transiently transfected with plasmid DNA expressing single
440 chain peptide-HLA-E-ß2m trimers so that they expressed HLA-E-RL9HIV, HLA-E-RL9SIV or
441 HLA-E-VL9 at the cell surface. Hybridomas cells that secreted HLA-E-VL9 antibodies were
442 cloned by limiting dilution for at least 5 rounds until the phenotypes of all limiting dilution wells
443 are identical. IgG mAbs were purified by protein G affinity chromatography, while IgM mAbs
444 were purified by ammonium sulfate precipitation and by Superose 6 column size-exclusion

chromatography in AKTA Fast Protein Liquid Chromatography (FPLC) system. The VH and VL sequences of mAbs were amplified from hybridoma cell RNA using primers reported previously (Tian et al., 2016; von Boehmer et al., 2016).

Cell Surface Staining and High-Throughput Screening (HTS)

HLA-E SCT constructs encoding HLA-E-VL9, HLA-E-RL9HIV, or HLA-E-RL9SIV were transfected into 293T cells using GeneJuice transfection reagent (Novagen, Catalog# 70967). For epitope mapping experiment, a panel of HLA-E-VL9 SCT constructs with single amino acid mutations were transfected into 293T cells using the same method. Cells were dissociated with 0.1% EDTA at 48 hours post-transfection and stained with a Fixable Near-IR Dead Cell Stain Kit (Thermo Fisher, Catalog# L34976). After washing, primary antibodies (supernatant from hybridoma cells, supernatant from transfected cells, or purified antibodies) were added and incubated with cells for 1 hour at 4°C, following by staining with 1:1000 diluted secondary antibodies for 30 mins at 4°C. For mouse primary antibodies, we used Alexa Fluor 555 (AF555) conjugated goat anti-mouse IgG (H+L) (Thermo Fisher, Catalog# A32727) or Alexa Fluor 647 (AF647) conjugated goat anti-mouse IgG (H+L) (Thermo Fisher, Catalog# A32728) as secondary antibodies; for human primary antibodies, we used AF555 conjugated goat anti-human IgG (H+L) (Thermo Fisher, Catalog# A-21433) or AF647 conjugated goat anti-human IgG (H+L) (Thermo Fisher, Catalog# A-21445) as secondary antibodies. Cells were then washed 3 times and resuspended in fixation buffer (1% formaldehyde in PBS, pH7.4). Data were acquired on a BD LSR II flow cytometer and analyzed using FlowJo version 10.

3H4 Fab production

A humanized version of the 3H4 antibody (3H4-huIgG1) was digested to produce Fab fragments using the Pierce Fab Preparation kit (ThermoFisher SCIENTIFIC). 3H4 Fab-retrieved sample was further purified by size exclusion on a Superdex S75 16/60 column and eluted into

PBS buffer. Following concentration to 1.1mg/mL and SDS-PAGE gel-based validation, 3H4 Fab purified material was incubated for 1 hours on ice with freshly purified HLA-E-VL9. The combined 3H4:Fab-HLA-E-VL9 sample was concentrated to 7.5mg/mL prior to crystallographic set-up.

Crystallization screening

Crystals were grown via sitting drop vapour-diffusion at 20 °C in a 200nL drop with a 1:1 protein to reservoir ratio (Walter et al., 2005). The 3H4 Fab-HLA-E(VL9) co-complex crystallized in 20% PEG 8000, 0.1 M Na HEPES at pH 7, in the ProPlex sparse matrix screen. Crystals were cryo-preserved in 25% glycerol and diffraction data were collected at the I03 beamline of Diamond Light Source.

Crystallographic analysis

Diffraction data were merged and indexed in xia2 dials (Winter et al., 2018). Outer shell reflections were excluded from further analysis to ensure the $CC_{1/2}$ value exceeded the minimum threshold (>0.5) in each shell (Karplus and Diederichs, 2012). Sequential molecular replacement was carried out in MolRep of the CCP4i suite using molecule one of the previously published Mtb44-bound HLA-E structure with the peptide coordinates deleted (PDB ID: 6GH4) and one molecule of the previously published anti-APP-tag Fab structure (PDB ID: 6HGU) as phasing models (Vagin and Teplyakov, 2010; Winn et al., 2011). Rigid body and retrained refinement were subsequently carried out by Phenix.refine (Afonine et al., 2012) in between manual model building in Coot (Emsley et al., 2010). Model geometry was validated by MolProbity (Chen et al., 2010) and structural interpretation was conducted using the PyMOL Molecular Graphics System, version 2.0 (Schrödinger, LLC) in addition to the PDBePISA (Krissinel and Henrick, 2007) and PDBeFOLD (Krissinel and Henrick, 2004) servers.

Antigen-Specific Single B Cell Sorting

HLA-E-VL9-specific human B cells were sorted in flow cytometry using a three-color sorting technique. Briefly, the stabilized HLA-E-β2M-peptide complexes were made as tetramers and conjugated with different fluorophores. Human pan-B cells, including naïve and memory B cells, were isolated from PBMCs of healthy donors using human pan-B cell enrichment kit (STEMCELL, Catalog# 19554). The isolated pan-B cells were then stained with IgM PerCp-Cy5.5 (Clone# G20-127, BD Biosciences, Catalog# 561285), IgD FITC (Clone# IA6-2, BD Biosciences, Catalog# 555778), CD3 PE-Cy5 (Clone# HIT3a, BD Biosciences, Catalog# 555341), CD235a PE-Cy5 (Clone# GA-R2, BD Biosciences, Catalog# 559944), CD10 PE-CF594 (Clone# HI10A, BD Biosciences, Catalog# 562396), CD27 PE-Cy7 (Clone# O323, eBioscience, Catalog# 25-0279), CD16 BV570 (Clone# 3G8, Biolegend, Catalog# 302035), CD14 BV605 (Clone# M5E2, Biolegend, Catalog# 301834), CD38 APC-AF700 (Clone# LS198-4-2, Beckman Coulter, Catalog# B23489), CD19 APC-Cy7 (Clone# LJ25C1, BD Biosciences, Catalog# 561743) and tetramers at 2 μg/million cells (including BV421-conjugated HLA-E-VL9 tetramer, PE-conjugated HLA-E-VL9 tetramer, APC-conjugated HLA-E-RL9SIV tetramer and APC-conjugated HLA-E-RL9HIV tetramer). The cells were then stained with a Fixable Aqua Dead Cell Stain Kit (Invitrogen, Catalog# L34957). HLA-E-VL9-specific B cells were sorted in BD FACSAria II flow cytometer (BD Biosciences) for viable $CD3^{neg}$/ $CD14^{neg}$ /$CD16^{neg}$ /$CD235a^{neg}$/$CD19^{pos}$ / HLA-E-$VL9^{double\text{-}pos}$/ HLA-E-$RL9HIV^{neg}$/HLA-E-$RL9SIV^{neg}$ subset as single cells in 96-well plates.

PCR Amplification of Human Antibody Genes

The $V_HD_HJ_H$ and V_LJ_L genes were amplified by RT-PCR from the flow cytometry-sorted single B cells using the methods as described previously (Liao et al., 2009; Wrammert et al., 2008) with modification. Primer details were listed in Tables S2. The PCR-amplified genes were then purified and sequenced with 10 μM forward and reverse primers. Sequences were

analyzed by using the human library in Clonalyst for the VDJ arrangements of the immunoglobulin *IGHV*, *IGKV*, and *IGLV* sequences and mutation frequencies (Kepler et al., 2014). Clonal relatedness of $V_HD_HJ_H$ and V_LJ_L sequences was determined as previously described (Liao et al., 2013).

Expression of $V_HD_HJ_H$ and V_LJ_L as Full-Length IgG Recombinant mAbs

Transient transfection of recombinant mAbs was performed as previously described (Liao et al., 2009). Briefly, purified PCR products were used for overlapping PCR to generate linear human antibody expression cassettes. The expression cassettes were transfected into 293i cells using ExpiFectamine (Thermo Fisher Scientific, Catalog# A14525). The supernatant samples containing recombinant antibodies were used for cell surface staining and HTS assay to measure the binding reactivities.

The selected human antibody genes were then synthesized and cloned (GenScript) in a human IgG1 backbone with 4A mutations to enhance antibody-dependent cell-mediated cytotoxicity (ADCC) or a human IgG2σ backbone with mutations that abolish ADCC (Saunders, 2019). Recombinant IgG mAbs were then produced in HEK293i suspension cells by transfection with ExpiFectamine and purified using Protein A resin. The purified mAbs were run in SDS-PAGE for Coomassie blue staining and western blot. Antibodies with aggregation were further purified in AKTA FPLC system using a Superdex 200 size-exclusion column.

Surface Plasmon Resonance (SPR)

Surface plasmon resonance assays were performed on a BIAcore 3000 instrument, and data analysis was performed with BIAevaluation 3.0 software as previously described (Liao et al., 2006). Briefly, streptavidin was directly immobilized to CM5 sensor chips, then biotinylated HLA-E-peptide complexes (HLA-E-VL9, HLA-E-RL9SIV, HLA-E-RL9HIV and mock control) were bound to the immobilized streptavidin. Purified mAbs flowed over CM5 sensor chips at

549 concentrations of 100 µg/ml, and antibody binding was monitored in real-time at 25°C with a
550 continuous flow of PBS at 30 µl/min.
551
552 **ELISA**
553 Direct binding ELISAs were conducted in 384-well ELISA plates coated with 2 µg/ml of C-
554 trap-stabilized HLA-E-VL9, C-trap-stabilized HLA-E-RL9HIV or C-trap-stabilized HLA-E-RL9SIV
555 in 0.1 M sodium bicarbonate overnight at 4°C. Plates were washed with PBS + 0.05% Tween 20
556 and blocked with 3% BSA in PBS at room temperature for 1 h. MAb samples were incubated for
557 1 h in 3-fold serial dilutions starting at 100 µg/ml, followed by washing with PBS-0.05% Tween
558 20. HRP-conjugated goat anti-human IgG secondary Ab (SouthernBiotech, catalog# 2040-05)
559 was diluted to 1: 10,000 in 1% BSA in PBS-0.05% Tween 20 and incubated at room
560 temperature for 1 h. For sandwich ELISA, 384-well ELISA plates were coated with HLA-E-VL9
561 antibodies in a 3-fold dilution starting from 100 µg/mL in 0.1 M sodium bicarbonate overnight at
562 4°C. Plates were washed with PBS + 0.05% Tween 20 and blocked with 3% BSA in PBS at
563 room temperature for 1 h. C-trap-stabilized HLA-E-VL9, C-trap-stabilized HLA-E-RL9HIV, C-
564 trap-stabilized HLA-E-RL9SIV, or diluent control were then added at 2 µg/mL and incubated at
565 room temperature for 1 h. After washing, HRP-conjugated anti-human β2M antibody (Biolegend,
566 catalog# 280303) were added at 0.2 µg/mL and incubated at room temperature for 1 h. These
567 plates were washed for 4 times and developed with tetramethylbenzidine substrate (SureBlue
568 Reserve). The reaction was stopped with 1 M HCl, and optical density at 450 nm (OD_{450}) was
569 determined.
570
571 **Antibody Poly-Reactivity Assays**
572 All mAbs isolated from mice and human were tested for ELISA binding to nine autoantigens
573 - Sjogren's syndrome antigen A (SSA), Sjogren's syndrome antigen (SSB), Smith antigen (Sm),
574 ribonucleoprotein (RNP), scleroderma 70 (Scl-70), Jo-1 antigen, double-stranded DNA

(dsDNA), centromere B (Cent B), and histone as previously described (Han et al., 2017; Liao et al., 2011). Indirect immunofluorescence assay of mAbs binding to HEp-2 cells (Inverness Medical Professional Diagnostics, Princeton, NJ) was performed as previously described (Haynes et al., 2005; Liao et al., 2011). MAbs 2F5 (Yang et al., 2013) and 17B (Moore and Sodroski, 1996) were used as positive and negative controls, respectively. All antibodies were screened in two independent experiments.

Negative Stain Electron Microscopy of IgM antibodies

FPLC purified IgM antibodies were diluted to 0.08 mg/ml in HEPES-buffered saline (pH 7.4) + 5% glycerol, and stained with 2% uranyl formate. Images were obtained with a Philips EM420 electron microscope at 82,000 magnification and processed in Relion 3.0.

Microbiome-derived Peptide Prediction

VL9 peptide sequence was first searched by similarity in NCBI microbial protein BLAST. The BLAST results were then analyzed for HLA-E binding epitope prediction using HLA class I peptide binding algorithms NetMHC 4.0 (Andreatta and Nielsen, 2016; Nielsen et al., 2003). Epitopes that have HLA-E binding prediction scores > 0.1, length = 9 aa, and are relative to human microbiome were synthesized for validation experiments.

Peptide-Pulsing in K562-E Cells

K562-E cells and K562-E/UL49.5 cells were resuspended with fresh IMDM media with 10% FBS at $2x10^6$ cells/ml. Peptides were added into cell suspension at a final concentration of 100 μM. The cell/peptide mixtures were incubated at 26°C with 5% CO_2 for 20-22 hours and were transferred to 37°C for 2 hours with 5% CO_2 before use. In the following mAb staining experiment, medium with 100 μM peptides was used to maintain peptide concentration.

NK Cell Cytotoxicity Assay

NK Cell Cytotoxicity was measured by ^{51}Cr release assay. Human NK-92 cells were used as effector cells in our study. Transfected 293T cells were used as target cells. Target cells were counted, washed, resuspended in R10 at 1×10^7 cell/ml, and labeled with $Na_2{}^{51}CrO_4$ at 250 µCi/ml for 2 hours at 37°C. After washing three times using R10, cells were mixed with effector cells in a final effector to target (E:T) ratio of 60:1 and 6:1 in triplicate wells in a flexible 96 well round bottom plates (PerkinElmer, Catalog# 1450-401). The plates were inserted in flexible 96-well plate cassettes (PerkinElmer, Catalog# 1450-101), sealed and incubated at 37°C for 4 hours. After the incubation, cells were pelleted by centrifugation, and from the top of the well, add 25 ul of supernatant to a rigid 96 well isoplates (PerkinElmer, Catalog#1450-514) containing 150 ul of Ultima Gold LSC Cocktail (Sigma, Catalog# L8286). The plates were inserted in rigid 96-well plate cassettes (PerkinElmer, Catalog# 1450-105), sealed and counted on Perkin Elmer Microbeta Triux 1450 counter. ^{51}Cr labeled target cells without effector cells were set as a spontaneous release control, and ^{51}Cr labeled target cells mixed with detergent (2% Triton X-100) were used as a maximum release control. The percentages of specific lysis were calculated with the formulation: The Percentages of Specific Lysis (^{51}Cr Release %) = [(Experimental Release – Spontaneous Release)/ (Maximum Release – Spontaneous Release)] x 100.

Statistics Analysis

Data were plotted using Prism GraphPad 8.0 or visualized using the ComplexHeatmap R package. Significant analysis was performed using two-tailed Mann-Whitney tests or chi-square test of independence to compare differences between groups with p-value < 0.05 considered significant.

ACKNOWLEDGMENTS

We thank Dr. Thorbald van Hall from Leiden University for kindly providing the K562-E cells and K562-E/UL49.5 cells. We thank Duke Human Vaccine Institute (DHVI) programs and finance staff for project oversight and the contributions of technical staff at the DHVI, including Jordan Cocchiaro, Kelly Soderberg, Ahmed Yousef Abuahmad, Yunfei Wang, Giovanna Hernandez, Esther Lee, Paige Power, Aja Sanzone, Brenna Harrington, Andrew Foulger, Amanda Newman, Cindy Bowman, Grace Stevens, Laura Sutherland, Margaret Deyton, Victoria Gee-Lai, Tarra Von Holle, Thad Gurley, Madison Berry, Kara Anasti, Katayoun Mansouri, Erika Dunford, and Dawn Jones Marshall. We thank the DHVI Flow Cytometry Core for technical assistance. This study was funded by the Collaboratory of AIDS Researchers for Eradication (CARE; UM1AI126619), the Center for HIV/AIDS Vaccine Immunology-Immunogen Discovery (CHAVI-ID; UMI-AI100645) grant and the Consortium for HIV/AIDS Vaccine Development grant (CHAVD; UM1AI144371) from NIH/NIAID/DAIDS, and the Bill and Melinda Gates Foundation OPP1108533.

AUTHOR CONTRIBUTIONS

D.L. immunized the mice, generated the hybridomas, sorted B cells, cloned the antibodies and analyzed data. S.B. made single-chain trimer constructs, performed epitope mapping experiments and analyzed data. G.G, L.W. and M.Q. prepared the antigens and HLA-E tetramers. L.W., G.G., D.R. and K.H performed structural experiments with oversight from E.Y.J.. D.W.C. helped with flow cytometry sorting set-up. R.S., R.P. and M.B. performed hybridoma experiments, ELISA assays and help with ^{51}Cr release assays. R.J.E. oversaw negative stain EM. M.A. supervised and interpreted the SPR experiments. K.W. oversaw and performed antibody gene sequence analysis. Z.M. and M.B. helped with antibody isolation. K.O.S. oversaw antigen production. P.B. provided advice on NK cell assays and contributed to

study design and data interpretation. B.F.H., G.G. D.L. and A.J.M. conceived, designed, coordinated the study. D.L. and B.F.H. wrote the manuscript which was reviewed by all authors.

DECLARATION OF INTERESTS

D.L., S.B., G.G., A.J.M. and B.F.H. have patents submitted on select aspects of the material in this paper.

REFERENCES

Afonine, P.V., Grosse-Kunstleve, R.W., Echols, N., Headd, J.J., Moriarty, N.W., Mustyakimov, M., Terwilliger, T.C., Urzhumtsev, A., Zwart, P.H., and Adams, P.D. (2012). Towards automated crystallographic structure refinement with phenix.refine. Acta Crystallogr D Biol Crystallogr *68*, 352-367.

Alberu, J., Morales-Buenrostro, L.E., de Leo, C., Vargas-Rojas, M.I., Marino-Vazquez, L.A., and Crispin, J.C. (2007). A non-allogeneic stimulus triggers the production of de novo HLA antibodies in healthy adults. Transpl Immunol *18*, 166-171.

Aldrich, C.J., DeCloux, A., Woods, A.S., Cotter, R.J., Soloski, M.J., and Forman, J. (1994). Identification of a Tap-dependent leader peptide recognized by alloreactive T cells specific for a class Ib antigen. Cell *79*, 649-658.

Andre, P., Brunet, C., Guia, S., Gallais, H., Sampol, J., Vivier, E., and Dignat-George, F. (1999). Differential regulation of killer cell Ig-like receptors and CD94 lectin-like dimers on NK and T lymphocytes from HIV-1-infected individuals. Eur J Immunol *29*, 1076-1085.

Andre, P., Denis, C., Soulas, C., Bourbon-Caillet, C., Lopez, J., Arnoux, T., Blery, M., Bonnafous, C., Gauthier, L., Morel, A.*, et al.* (2018). Anti-NKG2A mAb Is a Checkpoint Inhibitor that Promotes Anti-tumor Immunity by Unleashing Both T and NK Cells. Cell *175*, 1731-1743 e1713.

Andreatta, M., and Nielsen, M. (2016). Gapped sequence alignment using artificial neural networks: application to the MHC class I system. Bioinformatics *32*, 511-517.

Braud, V., Jones, E.Y., and McMichael, A. (1997). The human major histocompatibility complex class Ib molecule HLA-E binds signal sequence-derived peptides with primary anchor residues at positions 2 and 9. Eur J Immunol *27*, 1164-1169.

Braud, V.M., Allan, D.S., O'Callaghan, C.A., Soderstrom, K., D'Andrea, A., Ogg, G.S., Lazetic, S., Young, N.T., Bell, J.I., Phillips, J.H., *et al.* (1998). HLA-E binds to natural killer cell receptors CD94/NKG2A, B and C. Nature *391*, 795-799.

Brooks, A.G., Posch, P.E., Scorzelli, C.J., Borrego, F., and Coligan, J.E. (1997). NKG2A complexed with CD94 defines a novel inhibitory natural killer cell receptor. J Exp Med *185*, 795-800.

Chen, F., Zou, Z., Du, J., Su, S., Shao, J., Meng, F., Yang, J., Xu, Q., Ding, N., Yang, Y., *et al.* (2019). Neoantigen identification strategies enable personalized immunotherapy in refractory solid tumors. J Clin Invest *129*, 2056-2070.

Chen, H., Zhang, Y., Ye, A.Y., Du, Z., Xu, M., Lee, C.S., Hwang, J.K., Kyritsis, N., Ba, Z., Neuberg, D., *et al.* (2020). BCR selection and affinity maturation in Peyer's patch germinal centres. Nature *582*, 421-425.

Chen, V.B., Arendall, W.B., 3rd, Headd, J.J., Keedy, D.A., Immormino, R.M., Kapral, G.J., Murray, L.W., Richardson, J.S., and Richardson, D.C. (2010). MolProbity: all-atom structure validation for macromolecular crystallography. Acta Crystallogr D Biol Crystallogr *66*, 12-21.

Chiossone, L., Dumas, P.Y., Vienne, M., and Vivier, E. (2018). Natural killer cells and other innate lymphoid cells in cancer. Nat Rev Immunol *18*, 671-688.

Colonna, M., and Samaridis, J. (1995). Cloning of immunoglobulin-superfamily members associated with HLA-C and HLA-B recognition by human natural killer cells. Science *268*, 405-408.

Creelan, B.C., and Antonia, S.J. (2019). The NKG2A immune checkpoint - a new direction in cancer immunotherapy. Nat Rev Clin Oncol *16*, 277-278.

DeKosky, B.J., Kojima, T., Rodin, A., Charab, W., Ippolito, G.C., Ellington, A.D., and Georgiou, G. (2015). In-depth determination and analysis of the human paired heavy- and light-chain antibody repertoire. Nat Med *21*, 86-91.

DeKosky, B.J., Lungu, O.I., Park, D., Johnson, E.L., Charab, W., Chrysostomou, C., Kuroda, D., Ellington, A.D., Ippolito, G.C., Gray, J.J., *et al.* (2016). Large-scale sequence and structural comparisons of human naive and antigen-experienced antibody repertoires. Proc Natl Acad Sci U S A *113*, E2636-2645.

Emsley, P., Lohkamp, B., Scott, W.G., and Cowtan, K. (2010). Features and development of Coot. Acta Crystallogr D Biol Crystallogr *66*, 486-501.

Garcia-Garijo, A., Fajardo, C.A., and Gros, A. (2019). Determinants for Neoantigen Identification. Front Immunol *10*, 1392.

714 Giltiay, N.V., Giordano, D., and Clark, E.A. (2019). The Plasticity of Newly Formed B Cells. J
715 Immunol *203*, 3095-3104.
716 Guillerey, C., Huntington, N.D., and Smyth, M.J. (2016). Targeting natural killer cells in cancer
717 immunotherapy. Nat Immunol *17*, 1025-1036.
718 Han, Q., Williams, W.B., Saunders, K.O., Seaton, K.E., Wiehe, K.J., Vandergrift, N., Von Holle,
719 T.A., Trama, A.M., Parks, R.J., Luo, K.*, et al.* (2017). HIV DNA-Adenovirus Multiclade Envelope
720 Vaccine Induces gp41 Antibody Immunodominance in Rhesus Macaques. J Virol *91*.
721 Hansen, S.G., Wu, H.L., Burwitz, B.J., Hughes, C.M., Hammond, K.B., Ventura, A.B., Reed, J.S.,
722 Gilbride, R.M., Ainslie, E., Morrow, D.W.*, et al.* (2016). Broadly targeted CD8(+) T cell responses
723 restricted by major histocompatibility complex E. Science *351*, 714-720.
724 Haynes, B.F., Fleming, J., St Clair, E.W., Katinger, H., Stiegler, G., Kunert, R., Robinson, J.,
725 Scearce, R.M., Plonk, K., Staats, H.F.*, et al.* (2005). Cardiolipin polyspecific autoreactivity in two
726 broadly neutralizing HIV-1 antibodies. Science *308*, 1906-1908.
727 Hickey, M.J., Valenzuela, N.M., and Reed, E.F. (2016). Alloantibody Generation and Effector
728 Function Following Sensitization to Human Leukocyte Antigen. Front Immunol *7*, 30.
729 Holodick, N.E., Rodriguez-Zhurbenko, N., and Hernandez, A.M. (2017). Defining Natural
730 Antibodies. Front Immunol *8*, 872.
731 Hu, W., Wang, G., Huang, D., Sui, M., and Xu, Y. (2019). Cancer Immunotherapy Based on
732 Natural Killer Cells: Current Progress and New Opportunities. Front Immunol *10*, 1205.
733 Joosten, S.A., van Meijgaarden, K.E., van Weeren, P.C., Kazi, F., Geluk, A., Savage, N.D.,
734 Drijfhout, J.W., Flower, D.R., Hanekom, W.A., Klein, M.R.*, et al.* (2010). Mycobacterium
735 tuberculosis peptides presented by HLA-E molecules are targets for human CD8 T-cells with
736 cytotoxic as well as regulatory activity. PLoS Pathog *6*, e1000782.
737 Kaiser, B.K., Pizarro, J.C., Kerns, J., and Strong, R.K. (2008). Structural basis for NKG2A/CD94
738 recognition of HLA-E. Proc Natl Acad Sci U S A *105*, 6696-6701.
739 Karlhofer, F.M., Ribaudo, R.K., and Yokoyama, W.M. (1992). MHC class I alloantigen specificity
740 of Ly-49+ IL-2-activated natural killer cells. Nature *358*, 66-70.
741 Karplus, P.A., and Diederichs, K. (2012). Linking crystallographic model and data quality. Science
742 *336*, 1030-1033.
743 Kepler, T.B., Munshaw, S., Wiehe, K., Zhang, R., Yu, J.S., Woods, C.W., Denny, T.N., Tomaras,
744 G.D., Alam, S.M., Moody, M.A.*, et al.* (2014). Reconstructing a B-Cell Clonal Lineage. II. Mutation,
745 Selection, and Affinity Maturation. Front Immunol *5*, 170.
746 Kim, N., Lee, H.H., Lee, H.J., Choi, W.S., Lee, J., and Kim, H.S. (2019). Natural killer cells as a
747 promising therapeutic target for cancer immunotherapy. Arch Pharm Res *42*, 591-606.

748 Klingemann, H., Boissel, L., and Toneguzzo, F. (2016). Natural Killer Cells for Immunotherapy -
749 Advantages of the NK-92 Cell Line over Blood NK Cells. Front Immunol *7*, 91.
750 Kraemer, T., Blasczyk, R., and Bade-Doeding, C. (2014). HLA-E: a novel player for
751 histocompatibility. J Immunol Res *2014*, 352160.
752 Kraemer, T., Celik, A.A., Huyton, T., Kunze-Schumacher, H., Blasczyk, R., and Bade-Doding, C.
753 (2015). HLA-E: Presentation of a Broader Peptide Repertoire Impacts the Cellular Immune
754 Response-Implications on HSCT Outcome. Stem Cells Int *2015*, 346714.
755 Krissinel, E., and Henrick, K. (2004). Secondary-structure matching (SSM), a new tool for fast
756 protein structure alignment in three dimensions. Acta Crystallogr D Biol Crystallogr *60*, 2256-2268.
757 Krissinel, E., and Henrick, K. (2007). Inference of macromolecular assemblies from crystalline
758 state. J Mol Biol *372*, 774-797.
759 Lampen, M.H., Hassan, C., Sluijter, M., Geluk, A., Dijkman, K., Tjon, J.M., de Ru, A.H., van der
760 Burg, S.H., van Veelen, P.A., and van Hall, T. (2013). Alternative peptide repertoire of HLA-E
761 reveals a binding motif that is strikingly similar to HLA-A2. Mol Immunol *53*, 126-131.
762 Lee, N., Goodlett, D.R., Ishitani, A., Marquardt, H., and Geraghty, D.E. (1998a). HLA-E surface
763 expression depends on binding of TAP-dependent peptides derived from certain HLA class I
764 signal sequences. J Immunol *160*, 4951-4960.
765 Lee, N., Llano, M., Carretero, M., Ishitani, A., Navarro, F., Lopez-Botet, M., and Geraghty, D.E.
766 (1998b). HLA-E is a major ligand for the natural killer inhibitory receptor CD94/NKG2A. Proc Natl
767 Acad Sci U S A *95*, 5199-5204.
768 Liao, H.X., Chen, X., Munshaw, S., Zhang, R., Marshall, D.J., Vandergrift, N., Whitesides, J.F.,
769 Lu, X., Yu, J.S., Hwang, K.K.*, et al.* (2011). Initial antibodies binding to HIV-1 gp41 in acutely
770 infected subjects are polyreactive and highly mutated. J Exp Med *208*, 2237-2249.
771 Liao, H.X., Levesque, M.C., Nagel, A., Dixon, A., Zhang, R., Walter, E., Parks, R., Whitesides, J.,
772 Marshall, D.J., Hwang, K.K.*, et al.* (2009). High-throughput isolation of immunoglobulin genes
773 from single human B cells and expression as monoclonal antibodies. J Virol Methods *158*, 171-
774 179.
775 Liao, H.X., Lynch, R., Zhou, T., Gao, F., Alam, S.M., Boyd, S.D., Fire, A.Z., Roskin, K.M.,
776 Schramm, C.A., Zhang, Z.*, et al.* (2013). Co-evolution of a broadly neutralizing HIV-1 antibody
777 and founder virus. Nature *496*, 469-476.
778 Liao, H.X., Sutherland, L.L., Xia, S.M., Brock, M.E., Scearce, R.M., Vanleeuwen, S., Alam, S.M.,
779 McAdams, M., Weaver, E.A., Camacho, Z.*, et al.* (2006). A group M consensus envelope
780 glycoprotein induces antibodies that neutralize subsets of subtype B and C HIV-1 primary viruses.
781 Virology *353*, 268-282.

Lin, S.Y., Hameed, A., Liu, Y.C., Hsu, Y.H., Lai, W.A., and Young, C.C. (2013). Pseudomonas formosensis sp. nov., a gamma-proteobacteria isolated from food-waste compost in Taiwan. Int J Syst Evol Microbiol *63*, 3168-3174.

Ljunggren, H.G., and Karre, K. (1985). Host resistance directed selectively against H-2-deficient lymphoma variants. Analysis of the mechanism. J Exp Med *162*, 1745-1759.

Ljunggren, H.G., and Karre, K. (1990). In search of the 'missing self': MHC molecules and NK cell recognition. Immunol Today *11*, 237-244.

Llano, M., Lee, N., Navarro, F., Garcia, P., Albar, J.P., Geraghty, D.E., and Lopez-Botet, M. (1998). HLA-E-bound peptides influence recognition by inhibitory and triggering CD94/NKG2 receptors: preferential response to an HLA-G-derived nonamer. Eur J Immunol *28*, 2854-2863.

Lowry, L.E., and Zehring, W.A. (2017). Potentiation of Natural Killer Cells for Cancer Immunotherapy: A Review of Literature. Front Immunol *8*, 1061.

Mahapatra, S., Mace, E.M., Minard, C.G., Forbes, L.R., Vargas-Hernandez, A., Duryea, T.K., Makedonas, G., Banerjee, P.P., Shearer, W.T., and Orange, J.S. (2017). High-resolution phenotyping identifies NK cell subsets that distinguish healthy children from adults. PLoS One *12*, e0181134.

Marin, R., Ruiz-Cabello, F., Pedrinaci, S., Mendez, R., Jimenez, P., Geraghty, D.E., and Garrido, F. (2003). Analysis of HLA-E expression in human tumors. Immunogenetics *54*, 767-775.

McKenna, R.M., Takemoto, S.K., and Terasaki, P.I. (2000). Anti-HLA antibodies after solid organ transplantation. Transplantation *69*, 319-326.

McMurtrey, C., Harriff, M.J., Swarbrick, G.M., Duncan, A., Cansler, M., Null, M., Bardet, W., Jackson, K.W., Lewinsohn, D.A., Hildebrand, W.*, et al.* (2017). T cell recognition of Mycobacterium tuberculosis peptides presented by HLA-E derived from infected human cells. PLoS One *12*, e0188288.

Michaelsson, J., Teixeira de Matos, C., Achour, A., Lanier, L.L., Karre, K., and Soderstrom, K. (2002). A signal peptide derived from hsp60 binds HLA-E and interferes with CD94/NKG2A recognition. J Exp Med *196*, 1403-1414.

Moore, J.P., and Sodroski, J. (1996). Antibody cross-competition analysis of the human immunodeficiency virus type 1 gp120 exterior envelope glycoprotein. J Virol *70*, 1863-1872.

Morales-Buenrostro, L.E., Terasaki, P.I., Marino-Vazquez, L.A., Lee, J.H., El-Awar, N., and Alberu, J. (2008). "Natural" human leukocyte antigen antibodies found in nonalloimmunized healthy males. Transplantation *86*, 1111-1115.

New, J.S., King, R.G., and Kearney, J.F. (2016). Manipulation of the glycan-specific natural antibody repertoire for immunotherapy. Immunol Rev *270*, 32-50.

Nielsen, M., Lundegaard, C., Worning, P., Lauemoller, S.L., Lamberth, K., Buus, S., Brunak, S., and Lund, O. (2003). Reliable prediction of T-cell epitopes using neural networks with novel sequence representations. Protein Sci *12*, 1007-1017.

O'Callaghan, C.A., Tormo, J., Willcox, B.E., Braud, V.M., Jakobsen, B.K., Stuart, D.I., McMichael, A.J., Bell, J.I., and Jones, E.Y. (1998). Structural features impose tight peptide binding specificity in the nonclassical MHC molecule HLA-E. Mol Cell *1*, 531-541.

Pende, D., Falco, M., Vitale, M., Cantoni, C., Vitale, C., Munari, E., Bertaina, A., Moretta, F., Del Zotto, G., Pietra, G.*, et al.* (2019). Killer Ig-Like Receptors (KIRs): Their Role in NK Cell Modulation and Developments Leading to Their Clinical Exploitation. Front Immunol *10*, 1179.

Petrie, E.J., Clements, C.S., Lin, J., Sullivan, L.C., Johnson, D., Huyton, T., Heroux, A., Hoare, H.L., Beddoe, T., Reid, H.H.*, et al.* (2008). CD94-NKG2A recognition of human leukocyte antigen (HLA)-E bound to an HLA class I leader sequence. J Exp Med *205*, 725-735.

Raulet, D.H. (2006). Missing self recognition and self tolerance of natural killer (NK) cells. Semin Immunol *18*, 145-150.

Ravindranath, M.H., Kaneku, H., El-Awar, N., Morales-Buenrostro, L.E., and Terasaki, P.I. (2010a). Antibodies to HLA-E in nonalloimmunized males: pattern of HLA-Ia reactivity of anti-HLA-E-positive sera. J Immunol *185*, 1935-1948.

Ravindranath, M.H., Taniguchi, M., Chen, C.W., Ozawa, M., Kaneku, H., El-Awar, N., Cai, J., and Terasaki, P.I. (2010b). HLA-E monoclonal antibodies recognize shared peptide sequences on classical HLA class Ia: relevance to human natural HLA antibodies. Mol Immunol *47*, 1121-1131.

Rolle, A., Meyer, M., Calderazzo, S., Jager, D., and Momburg, F. (2018). Distinct HLA-E Peptide Complexes Modify Antibody-Driven Effector Functions of Adaptive NK Cells. Cell Rep *24*, 1967-1976 e1964.

Sanchez, A.M., DeMarco, C.T., Hora, B., Keinonen, S., Chen, Y., Brinkley, C., Stone, M., Tobler, L., Keating, S., Schito, M.*, et al.* (2014a). Development of a contemporary globally diverse HIV viral panel by the EQAPOL program. J Immunol Methods *409*, 117-130.

Sanchez, A.M., Rountree, W., Berrong, M., Garcia, A., Schuetz, A., Cox, J., Frahm, N., Manak, M., Sarzotti-Kelsoe, M., D'Souza, M.P.*, et al.* (2014b). The External Quality Assurance Oversight Laboratory (EQAPOL) proficiency program for IFN-gamma enzyme-linked immunospot (IFN-gamma ELISpot) assay. J Immunol Methods *409*, 31-43.

Saunders, K.O. (2019). Conceptual Approaches to Modulating Antibody Effector Functions and Circulation Half-Life. Front Immunol *10*, 1296.

Sensi, M., Pietra, G., Molla, A., Nicolini, G., Vegetti, C., Bersani, I., Millo, E., Weiss, E., Moretta, L., Mingari, M.C.*, et al.* (2009). Peptides with dual binding specificity for HLA-A2 and HLA-E are

encoded by alternatively spliced isoforms of the antioxidant enzyme peroxiredoxin 5. Int Immunol *21*, 257-268.

Souza-Fonseca-Guimaraes, F., Cursons, J., and Huntington, N.D. (2019). The Emergence of Natural Killer Cells as a Major Target in Cancer Immunotherapy. Trends Immunol *40*, 142-158.

Sullivan, L.C., Westall, G.P., Widjaja, J.M., Mifsud, N.A., Nguyen, T.H., Meehan, A.C., Kotsimbos, T.C., and Brooks, A.G. (2015). The Presence of HLA-E-Restricted, CMV-Specific CD8+ T Cells in the Blood of Lung Transplant Recipients Correlates with Chronic Allograft Rejection. PLoS One *10*, e0135972.

Taurog, J., Hammer, R., Maika, S., Sams, K., El-Zaatari, F., Stimpson, S., and Schwab, J. (1990). HLA-B27 transgenic mice as potential models of human disease. In Transgenic mice and mutants in MHC research (Springer), pp. 268-275.

Tian, M., Cheng, C., Chen, X., Duan, H., Cheng, H.L., Dao, M., Sheng, Z., Kimble, M., Wang, L., Lin, S.*, et al.* (2016). Induction of HIV Neutralizing Antibody Lineages in Mice with Diverse Precursor Repertoires. Cell *166*, 1471-1484 e1418.

Tomasec, P., Braud, V.M., Rickards, C., Powell, M.B., McSharry, B.P., Gadola, S., Cerundolo, V., Borysiewicz, L.K., McMichael, A.J., and Wilkinson, G.W. (2000). Surface expression of HLA-E, an inhibitor of natural killer cells, enhanced by human cytomegalovirus gpUL40. Science *287*, 1031.

Vagin, A., and Teplyakov, A. (2010). Molecular replacement with MOLREP. Acta Crystallogr D Biol Crystallogr *66*, 22-25.

van Hall, T., Andre, P., Horowitz, A., Ruan, D.F., Borst, L., Zerbib, R., Narni-Mancinelli, E., van der Burg, S.H., and Vivier, E. (2019). Monalizumab: inhibiting the novel immune checkpoint NKG2A. J Immunother Cancer *7*, 263.

van Meijgaarden, K.E., Haks, M.C., Caccamo, N., Dieli, F., Ottenhoff, T.H., and Joosten, S.A. (2015). Human CD8+ T-cells recognizing peptides from Mycobacterium tuberculosis (Mtb) presented by HLA-E have an unorthodox Th2-like, multifunctional, Mtb inhibitory phenotype and represent a novel human T-cell subset. PLoS Pathog *11*, e1004671.

van Montfoort, N., Borst, L., Korrer, M.J., Sluijter, M., Marijt, K.A., Santegoets, S.J., van Ham, V.J., Ehsan, I., Charoentong, P., Andre, P.*, et al.* (2018). NKG2A Blockade Potentiates CD8 T Cell Immunity Induced by Cancer Vaccines. Cell *175*, 1744-1755 e1715.

von Boehmer, L., Liu, C., Ackerman, S., Gitlin, A.D., Wang, Q., Gazumyan, A., and Nussenzweig, M.C. (2016). Sequencing and cloning of antigen-specific antibodies from mouse memory B cells. Nat Protoc *11*, 1908-1923.

Walter, T.S., Diprose, J.M., Mayo, C.J., Siebold, C., Pickford, M.G., Carter, L., Sutton, G.C., Berrow, N.S., Brown, J., Berry, I.M., *et al.* (2005). A procedure for setting up high-throughput nanolitre crystallization experiments. Crystallization workflow for initial screening, automated storage, imaging and optimization. Acta Crystallogr D Biol Crystallogr *61*, 651-657.

Walters, L.C., Harlos, K., Brackenridge, S., Rozbesky, D., Barrett, J.R., Jain, V., Walter, T.S., O'Callaghan, C.A., Borrow, P., Toebes, M., *et al.* (2018). Pathogen-derived HLA-E bound epitopes reveal broad primary anchor pocket tolerability and conformationally malleable peptide binding. Nat Commun *9*, 3137.

Walters, L.C., McMichael, A.J., and Gillespie, G.M. (2020). Detailed and atypical HLA-E peptide binding motifs revealed by a novel peptide exchange binding assay. Eur J Immunol.

Winn, M.D., Ballard, C.C., Cowtan, K.D., Dodson, E.J., Emsley, P., Evans, P.R., Keegan, R.M., Krissinel, E.B., Leslie, A.G., McCoy, A., *et al.* (2011). Overview of the CCP4 suite and current developments. Acta Crystallogr D Biol Crystallogr *67*, 235-242.

Winter, G., Waterman, D.G., Parkhurst, J.M., Brewster, A.S., Gildea, R.J., Gerstel, M., Fuentes-Montero, L., Vollmar, M., Michels-Clark, T., Young, I.D., *et al.* (2018). DIALS: implementation and evaluation of a new integration package. Acta Crystallogr D Struct Biol *74*, 85-97.

Wrammert, J., Smith, K., Miller, J., Langley, W.A., Kokko, K., Larsen, C., Zheng, N.Y., Mays, I., Garman, L., Helms, C., *et al.* (2008). Rapid cloning of high-affinity human monoclonal antibodies against influenza virus. Nature *453*, 667-671.

Yang, G., Holl, T.M., Liu, Y., Li, Y., Lu, X., Nicely, N.I., Kepler, T.B., Alam, S.M., Liao, H.X., Cain, D.W., *et al.* (2013). Identification of autoantigens recognized by the 2F5 and 4E10 broadly neutralizing HIV-1 antibodies. J Exp Med *210*, 241-256.

Yokoyama, W.M., and Kim, S. (2006). How do natural killer cells find self to achieve tolerance? Immunity *24*, 249-257.

Yu, Y.Y., Netuschil, N., Lybarger, L., Connolly, J.M., and Hansen, T.H. (2002). Cutting edge: single-chain trimers of MHC class I molecules form stable structures that potently stimulate antigen-specific T cells and B cells. J Immunol *168*, 3145-3149.

912 **FIGURES**

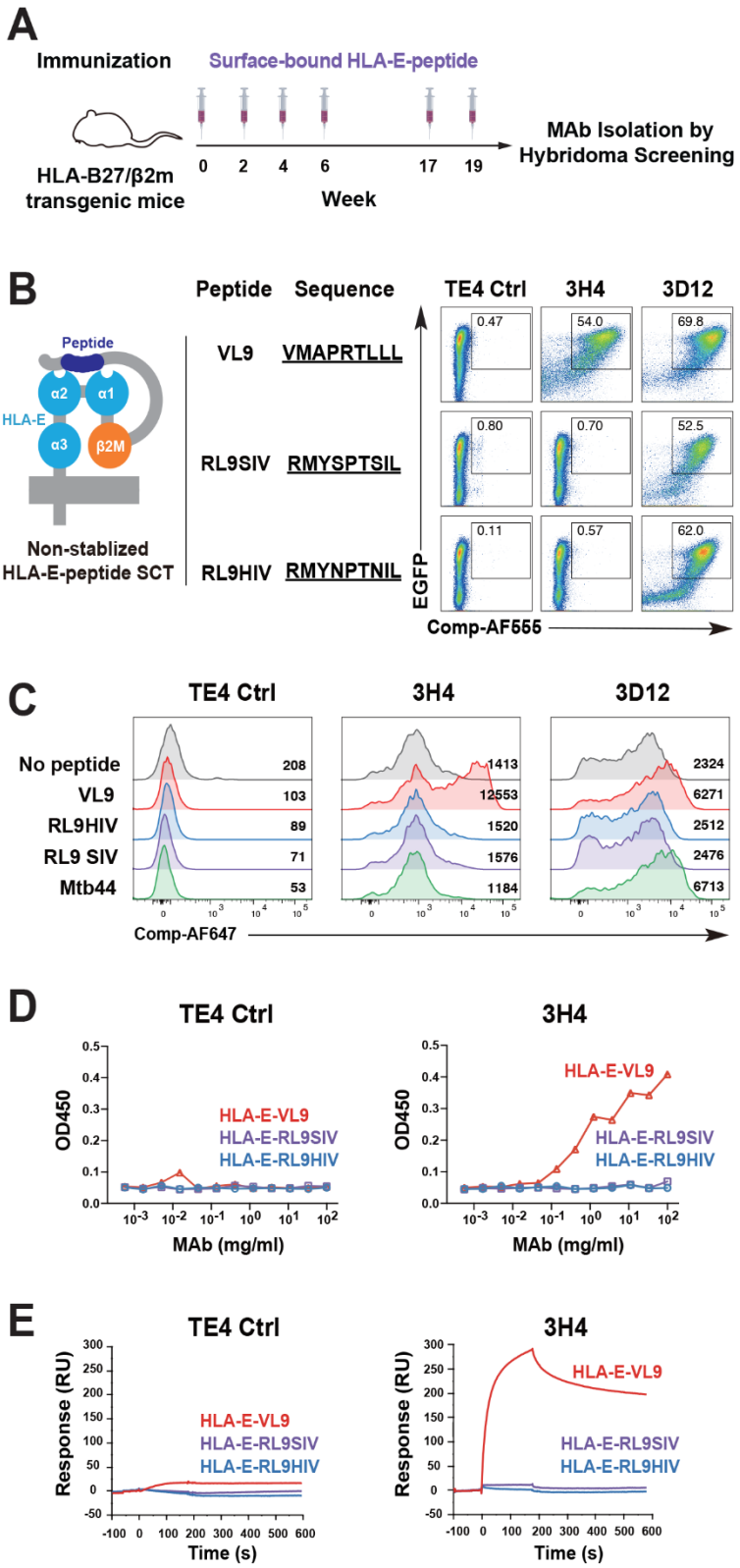

913

914 **Figure 1. Isolation of monoclonal antibodies specifically targeting HLA-E-VL9 complex.**

915 **(A) HLA-E specific antibodies elicited by vaccination.** HLA-B27/β2M transgenic (TG) mice

916 (*n*=10) were used to minimize the induction of antibodies to HLA class I and β2M. Animals were

917 immunized with cell surface-expressing HLA-E-RL9 peptide (a peptide derived from HIV-1;

918 denoted RL9HIV hereafter) single-chain trimer (SCT)-transfected 293T cells (indicated by red

919 arrows).

920 **(B) 3H4 bound HLA-E-VL9 SCT-transfected 293T cells.** All SCT constructs express EGFP to

921 indicate transfection efficiency. Transfected cells were stained with testing antibody and then an

922 Alexa fluor 555 (AF555)-anti-mouse Ig(H+L) secondary antibody. A control mouse IgM TE4 was

923 used as a negative control. Anti-pan-HLA-E antibody 3D12 was used as a positive control.

924 **(C) 3H4 bound VL9 peptide pulsed K562-HLA-E cells.** RL9HIV, RL9SIV, Mtb44 peptides

925 served as peptide controls. TE4 and 3D12 were used as antibody controls. Peptide-pulsed cells

926 were stained with testing antibody and then an Alexa fluor 647 (AF647)-anti-mouse Ig(H+L)

927 secondary antibody. Mean fluorescence intensity (MFI) of each sample is shown.

928 **(D-E) 3H4 specifically bound to soluble HLA-E-VL9 complexes as measured by ELISA**

929 **and SPR**. (D) ELISA plates were coated with 3H4 or control IgM TE4 in serial dilution, blocked,

930 and incubated with C-trap-stabilized HLA-E-VL9, HLA-E-RL9HIV, HLA-E-RL9SIV antigens.

931 After washing, antigen binding was detected by adding HRP-conjugated anti-human β2M

932 antibody. (E) For SPR, biotinylated HLA-E-peptide complexes (HLA-E-VL9, HLA-E-RL9SIV,

933 HLA-E-RL9HIV and mock control) were bound to the immobilized streptavidin. Antibody 3H4

934 and control TE4 were flowed over sensor chips and antibody binding was monitored in real-

935 time.

936

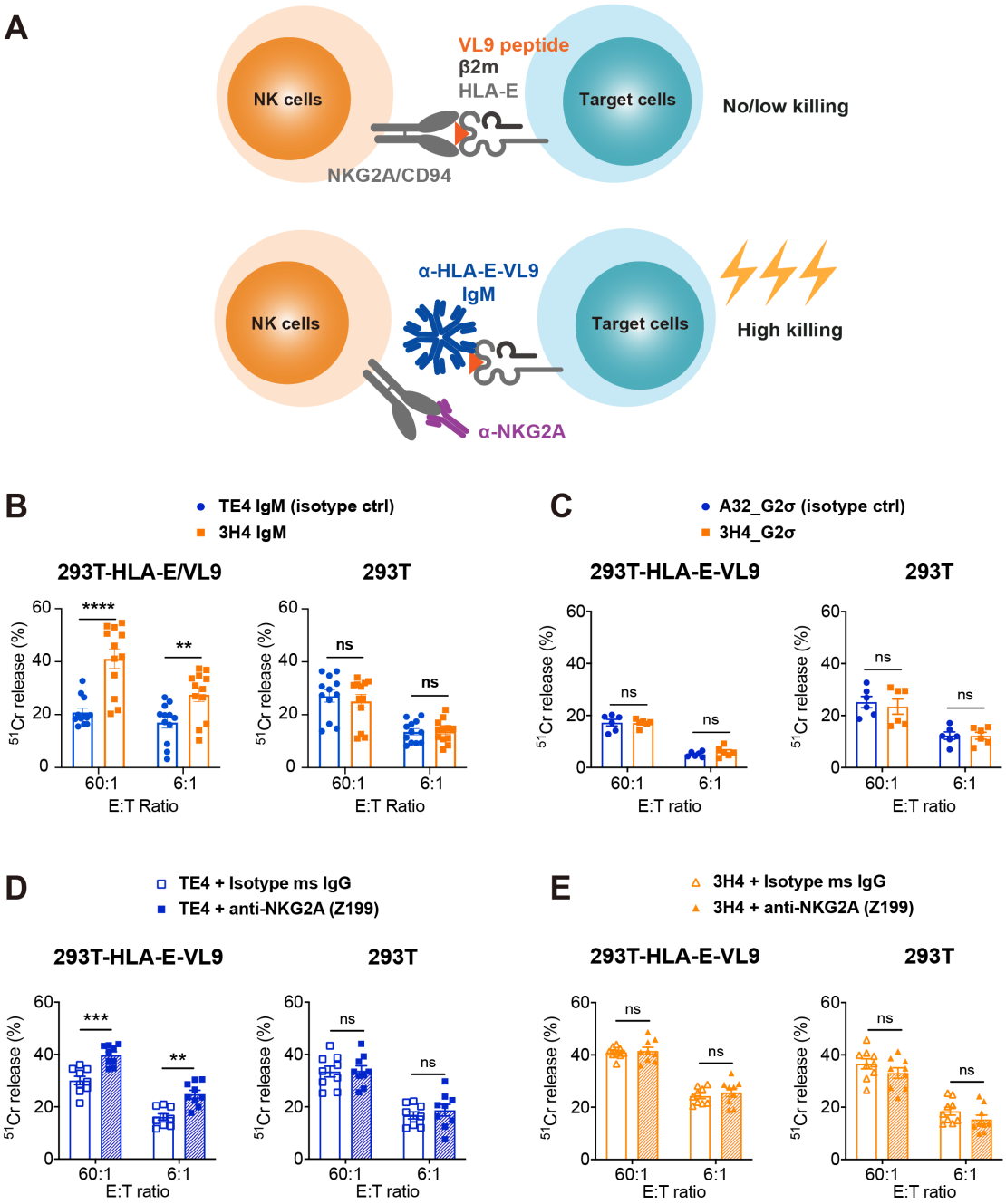

Figure 2. MAb 3H4 enhances cytotoxicity of a NKG2A+ NK cell line against HLA-E-VL9 expressing cells.

(A) Schematic graph of the hypothesis. Blockade of the inhibitory NKG2A/CD94/HLA-E pathway with anti-HLA-E-VL9 antibody (3H4) and/or anti-NKG2A antibody (Z199) could enhance target cell lysis by NK cells.

(B-C) NK cell cytotoxicity against 3H4 IgM (B) or 3H4 IgG (C) treated target cells as assessed by ^{51}Cr release assay. Antibody was incubated with HLA-E-VL9 transfected 293T cells and untransfected 293T cells at final concentration of 10 μg/ml, and NK92 cells were added into the mixture as effector cells. Mouse IgM TE4 or human IgG A32_G2σ were used as isotype controls. Dots represent all the data from four independent experiments, and bars show mean ± SEM.

(D-E) NK cell cytotoxicity in the presence of anti-NKG2A mouse IgG Z199 in combination with TE4 control- or 3H4- treated target cells as assessed by ^{51}Cr release assay. Antibody combinations of Z199 + TE4 control (D) or Z199 + 3H4 (E) were incubated with HLA-E-VL9 transfected 293T cells and untransfected 293T cells at a final concentration of 10 μg/ml, and NK92 cells were added into the mixture as effector cells. Dots represent all the data from three independent experiments, and bars show mean ± SEM.

The p-values in all the panels were determined by Mann-Whitney U tests. ****, $p<0.0001$; ***, $0.0001<p<0.001$; **, $0.001<p<0.01$; ns, not significant.

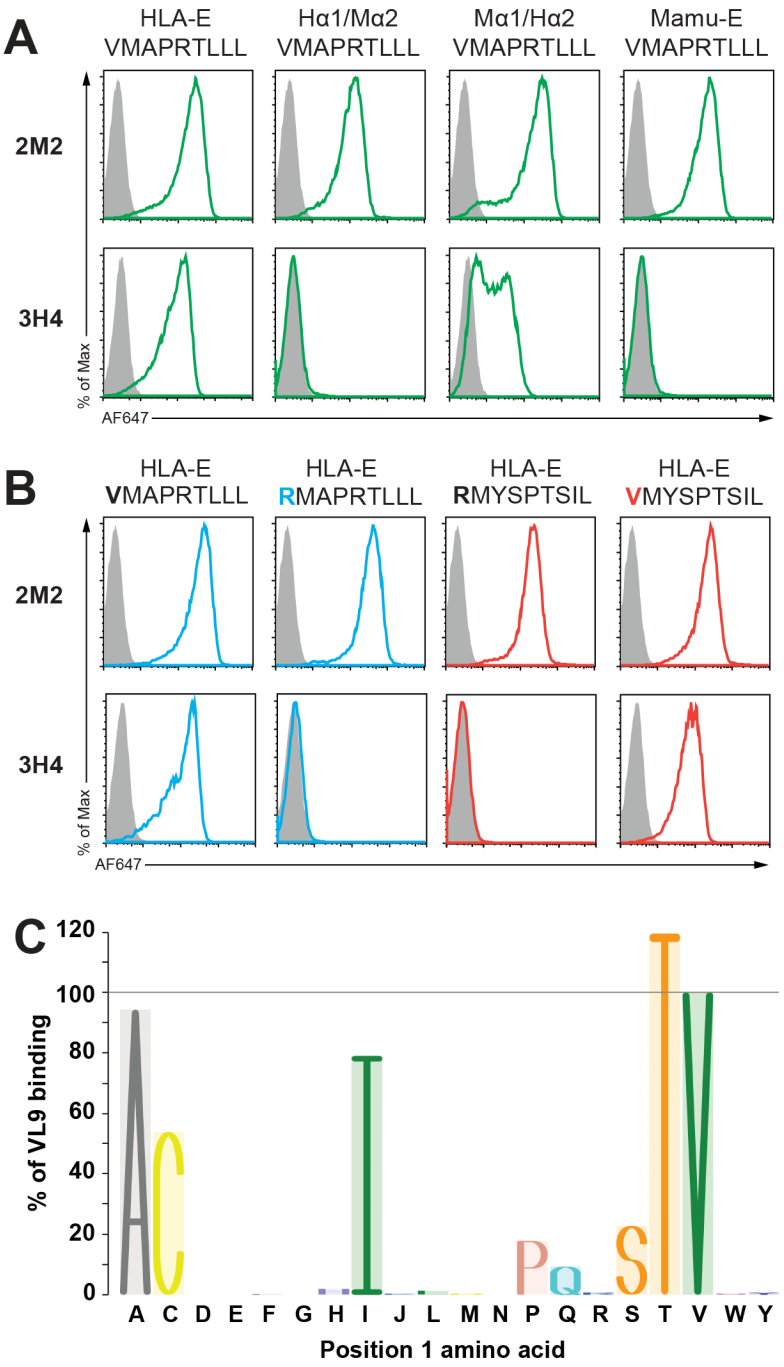

Figure 3. 3H4 recognition of both the HLA-E heavy chain α2 domain and the VL9 peptide.

(A) 3H4 recognizes the α2 domain of HLA-E. Flow cytometry analysis of 3H4 and 4D12 (HLA-E mAb) binding to 293T cells transfected with VL9 presented by HLA-E, Mamu-E, and two HLA-E/Mamu-E hybrids - one with HLA-E α1/Mamu-E α2 (Hα1/Mα2), the other with Mamu-E α1/HLA-E α2 (Mα1/Hα2) (green). Transfected cells were stained with testing antibody and then

an AF647-anti-mouse Ig(H+L) secondary antibody. Isotype control stained cells were used as negative controls (grey filled histograms).

(B) 3H4 recognizes position 1 (P1) of the VL9 peptide. 3H4 and 2M2 (a control β2M mAb) staining of 293T cells transfected with HLA-E-VL9 (VMAPRTLLL) or HLA-E-VL9 with a mutation at P1 (valine to arginine; RMAPRTLLL) (blue), and with HLA-E-RL9HIV (RMYSPTSIL) or HLA-E-RL9HIV with a mutation at P1 (arginine to valine; VMYSPTSIL) (red). Transfected cells were stained with testing antibody and then an AF647-anti-mouse Ig(H+L) secondary antibody. Isotype control stained cells used as negative controls (grey filled histograms).

(C) 3H4 recognizes peptides with variants in P1. 293T cells were transfected with HLA-E SCTs with VL9 peptides with single amino acid mutations at P1, then stained with 3H4 antibody followed by AF647 conjugated anti-mouse IgG(H+L) secondary antibody. Cells were gated for EGFP positive subsets. MFI of 3H4 staining on wildtype VL9 peptide was set as 100%, and the percentages equals to (MFI of 3H4 binding on each P1 variant) / (MFI of 3H4 binding on wildtype VL9) x 100%.

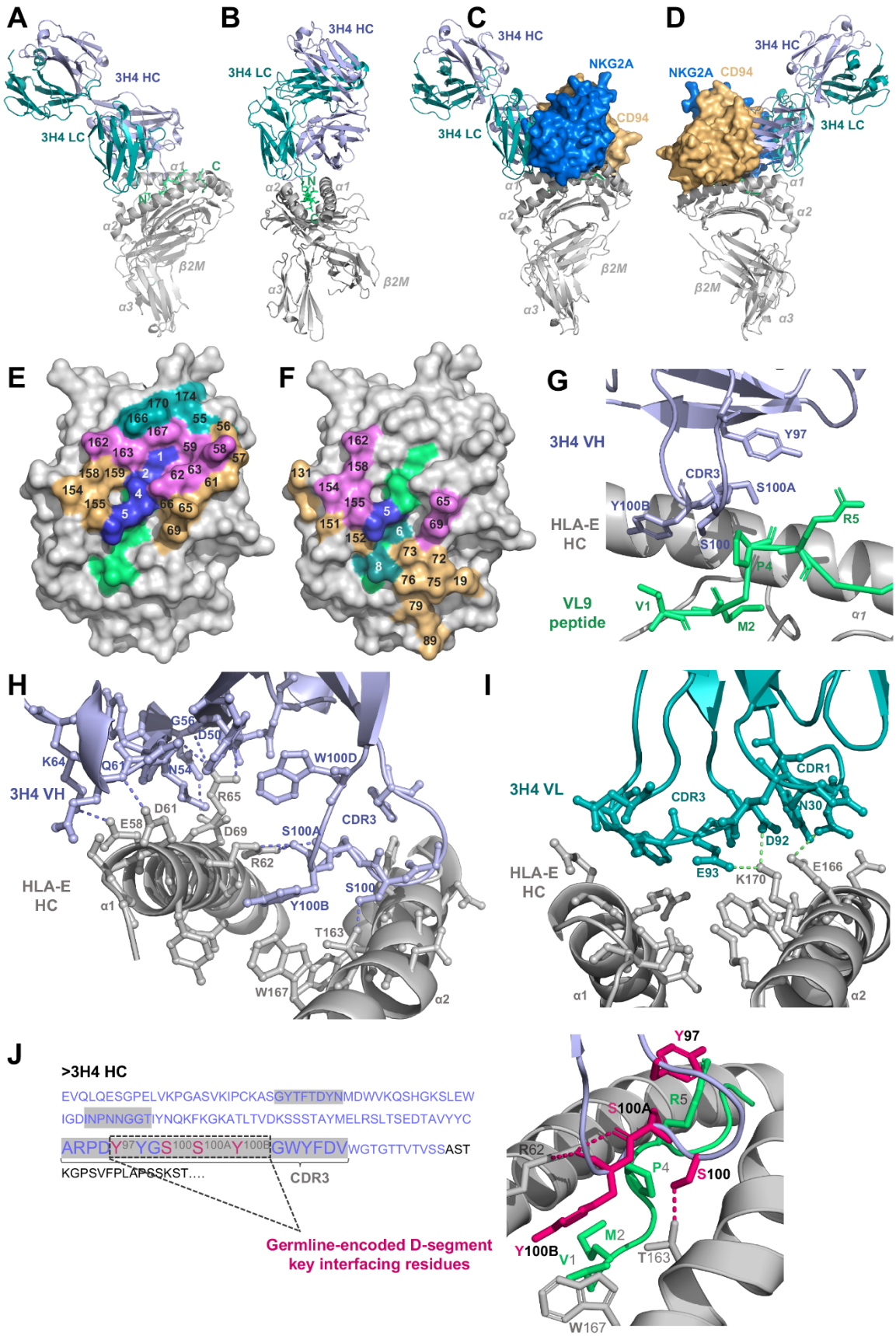

978

Figure 4. 3H4 Fab-HLA-E-VL9 co-complex structural visualisation.

(A-B) 3H4 Fab-HLA-E docking angles. The HLA-E heavy chain and β2M light chain are shown as a grey cartoon, the VL9 peptide as lime green sticks, the 3H4 HC as a light purple cartoon and the 3H4 light chain (LC) as a teal cartoon.

(C-D) Superposition of 3H4 Fab and CD94/NKG2A docking sites on HLA-E. The HLA-E complex and 3H4 Fab are color-coded according to A and B. The CD94 subunit is shown as an orange surface and the NKG2A subunit as a marine blue surface.

(E) Aerial view of the HLA-E-VL9 peptide binding groove surface. Non-interfacing residues of the HLA-E heavy chain are shaded light grey and non-interfacing peptide residues shaded lime green. VL9 peptide residues involved in the 3H4 interface are coloured marine blue. Interfacing HLA-E HC residues that contact the 3H4 VH are shaded orange whereas those that contact the 3H4 VL are shaded teal. HLA-E heavy chain residues involved in the interface with both the 3H4 VH and VL are shaded violet. Residue positions are numbered on the HLA-E surface view.

(F) Aerial view of the overlapping 3H4 and CD94/NKG2A footprints on the HLA-E peptide binding groove. VL9 peptide residues involved in both the 3H4 and CD94/NKG2A interfaces are shaded marine blue whereas HLA-E heavy chain residues involved in both interfaces are shaded violet. Peptide and HLA-E heavy chain residues involved exclusively in the CD94/NKG2A interface are shaded in teal and orange, respectively.

(G) Binding interface of 3H4 HC/VL9 peptide. Interfacing residues (Y97, S100, S100A and Y100B of the VH CDR3 loop and V1, M2, P4 and R5 of the VL9 peptide) are shown in ball and stick-form with non-interfacing residues in cartoon form. The VL9 peptide is shaded lime green, the HLA-E heavy chain in grey and the 3H4 HC in light purple. 3H4 is numbered according to the Kabat scheme whereby alternate insertion codes (letters after the residue number) are added to variable length regions of the antibody sequence. Kabat numbering is applied in all subsequent figures.

(H-I) Binding interfaces of 3H4 HC/HLA-E heavy chain (H) and 3H4 LC/HLA-E HC (I). Interfacing residues are displayed in ball-and-stick form, non-interfacing residues are displayed in cartoon form and hydrogen bonds as dashed lines. In the 3H4 HC/HLA-E heavy chain interface (H), interfacing residues derived from the HLA-E heavy chain (grey) include G56, S57, E58, Y59, D61, R62, E63, R65, S66 and D69 of the α1-helix and E154, H155, A158, Y159, D162, T163 and W167 of the α2-helix. 3H4 VH (light purple) interfacing residues include N33 of the CDR1 region, N52, N54, G56 and T57 of the CDR2 region, Y97, G99, S100, S100A, Y100B and W100D of the CDR3 region and W47, D50, I58, Y59, N60, Q61 and K64 of the non-CDR VH domain. In the 3H4 LC/HLA-E heavy chain interface (I), HLA-E heavy chain (grey)-derived interfacing residues include E55, E58, Y59 and R62 of the α1-helix and D162, T163, E166, W167, K170 and K174 of the α2-helix. 3H4 LC (teal) interfacing residues include Q27, D28, N30 and Y32 of the CDR1 region, D92, E93, F94 and P95 of the CDR3 region in addition to D1 of the VL domain.

(J) Key interfacing residues within the germline-encoded D-junction. 3H4 HC amino acid sequence with the VH segment in purple and the CDR1/2/3 regions shaded grey. Germline-encoded residues within the VH CDR3 D-junction are denoted. The 4 key interfacing residues (Y97, S100, S100A and Y100B) within this germline-encoded D-junction that make contacts with both the HLA-E heavy chain and VL9 peptide are highlighted magenta in the sequence and illustrated as magenta sticks in the PyMol visualisation. The HLA-E heavy chain and VL9 peptide are displayed as grey and green cartoons, respectively, with key interfacing residues in stick form. Hydrogen bonds are depicted as magenta dashed lines and residues of the 3H4 VH domain that are not germline-encoded key interfacing residues are displayed in light purple cartoon form.

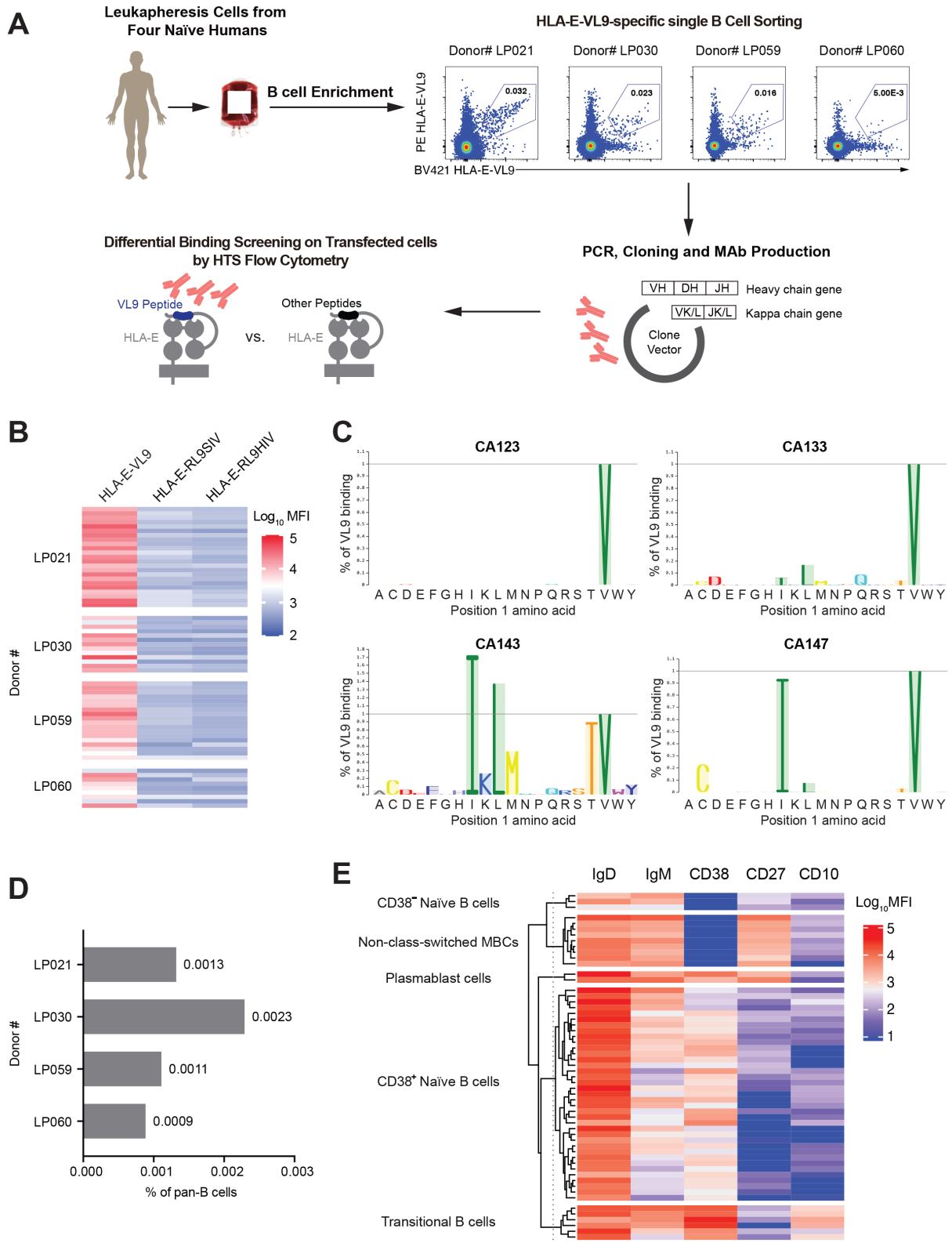

Figure 5. HLA-E-VL9-specific antibodies exist in the B cell pool of healthy humans.

(A) Scheme of isolating HLA-E-VL9-specific antibodies from healthy humans. Pan-B cells were first isolated by negative selection from human leukapheresis PBMCs. A three-color sorting strategy was used to sort single B cells that were positive for HLA-E-VL9 and negative for HLA-E-RL9HIV or HLA-E-RL9SIV. Flow cytometry data showing the sorting of HLA-E-VL9 double positive, HLA-E-RL9HIV negative, HLA-E-RL9SIV negative B cells in PBMCs from four donors (LP021, LP030, LP059 and LP060) are shown. Viable regions of antibody heavy and light chain genes were isolated from the sorted B cells by PCR, and constructed into an expression backbone with a human IgG1 constant region. Antibodies were produced by transient transfection in 293i cells, and antibody binding specificities were analyzed by surface staining of transfected 293T cells and high throughput screening (HTS) flow cytometry.

(B) Binding specificities of the HLA-E-VL9-specific antibodies (*n*=56) from four different donors shown as a heatmap. The compensated MFIs of HLA-E-VL9-specific antibodies staining on transfected 293T cells at the concentration of 1 μg/ml were shown.

(C) Mapping of representative HLA-E-VL9-specific mAbs CA123, CA133, CA143 and CA147 on 293T cells transfected with HLA-E-VL9 peptide variants. 293T cells were transfected with HLA-E SCTs with VL9 peptides with single amino acid mutations at P1, then stained with human antibodies CA123, CA133, CA143, and CA147, followed by AF647 conjugated anti-mouse IgG(H+L) secondary antibody (dark blue). Cells were gated for EGFP positive subsets. MFI of the indicated antibody staining on wildtype VL9 peptide was set as 100%, and the percentages equals to (MFI of binding on each P1 variant) / (MFI of binding on wildtype VL9) x 100%.

(D) Percentage of HLA-E-VL9-specific B cells in CD19^{+} pan-B cells in four donors.

(E) Phenotypes of HLA-E-VL9-specific B cells (*n*=56) shown as heatmap. Expression of markers in each single B cell were determined from index sorting data and are shown as MFIs after compensation. Compensated MFIs below zero were set as zero. Each row indicates one single cell. The rows were clustered by K-means Clustering in R. Four subsets were observed:

1057 $CD10^{-}CD27^{-}CD38^{+/-}$ naïve B cells, $CD10^{+}CD27^{-}CD38^{++}$ transitional B cells, $CD10^{-}CD27^{+}CD38^{-}$

1058 non-class-switched memory B cells, and $CD10^{-}CD27^{+}CD38^{+}$ plasmablast cells. Detailed

1059 information for each single cell and antibody is shown in ***Table S6***.

1060

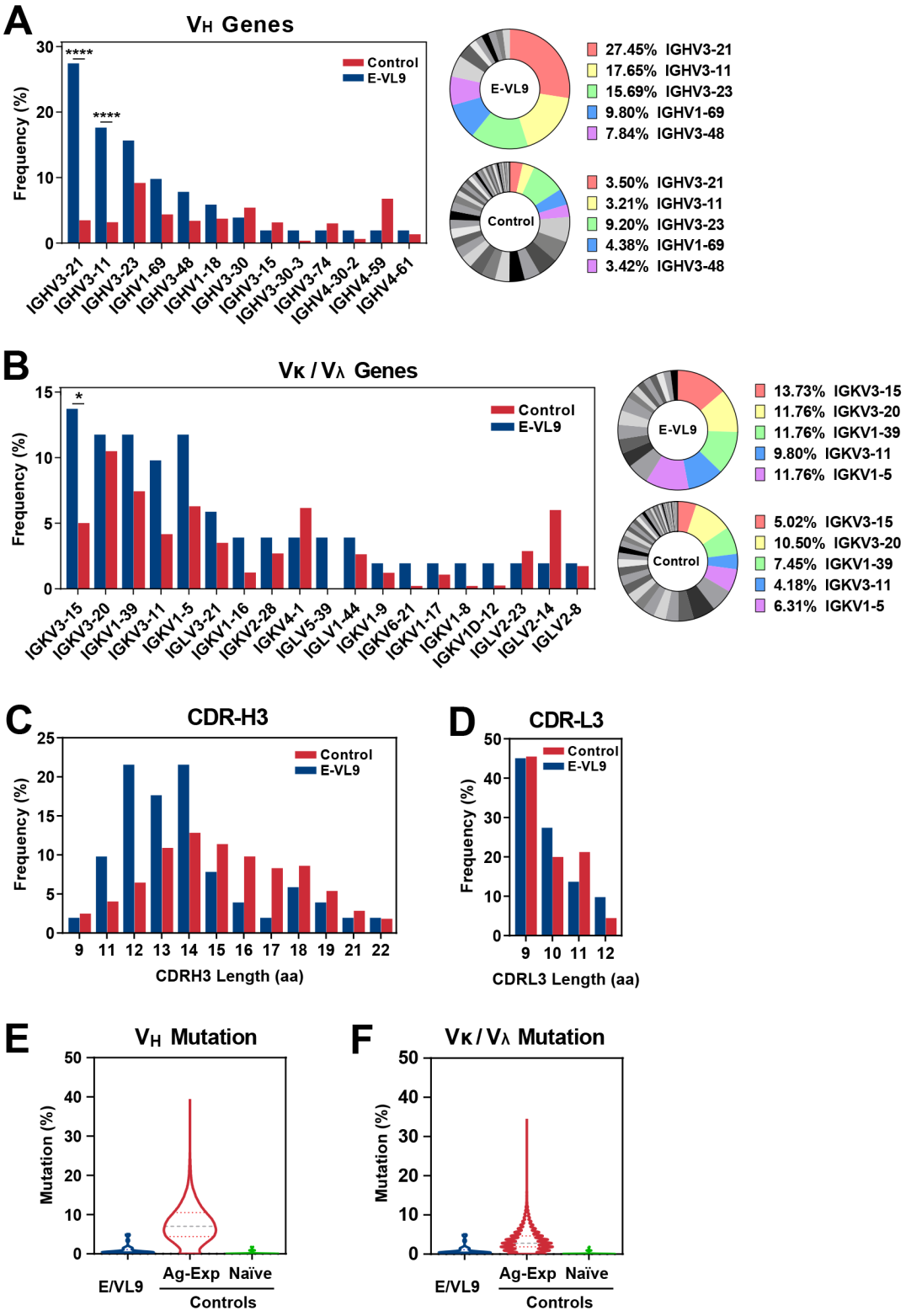

Figure 6. Sequence analysis of HLA-E-VL9-specific antibodies. HLA-E-VL9-specific antibody (n=51) genes isolated from healthy humans were analyzed by Clonalyst and corrected

for clonality. Reference VH-VL repertoires (n=198,148) from three healthy humans from a previous study (DeKosky et al., 2015) was used as a control for panels A-D Another set of reference sequences comparing naïve and antigen-experienced (Ag-Exp) antibody repertoires (n=13,780 and 34,692, respectively) (DeKosky et al., 2016) was used as a control for panel E-F. The chi-square test of independence was performed to test for an association between indicated gene usage and repertoire/antibody type in panels A-B. ****, $p<0.0001$; *, $0.01<p<0.05$.

(A) Heavy chain viable (V_H) region gene usage shown as a bar chart (left) and pie chart (right). The top five V_H genes found in HLA-E-VL9-specific antibodies are colored in the pie charts.

(B) Kappa chain variable (V_κ) and lambda chain variable (V_λ) region gene usage shown as a bar chart (left) and pie chart (right). The top five V_κ/V_λ genes found in HLA-E-VL9-specific antibodies are colored in the pie charts.

(C) Comparison of heavy chain CDR3 (CDR-H3) length.

(D) Comparison of light chain CDR3 (CDR-L3) length.

(E-F) Violin plots showing the mutation rates of heavy chains (H) and light chains (I).

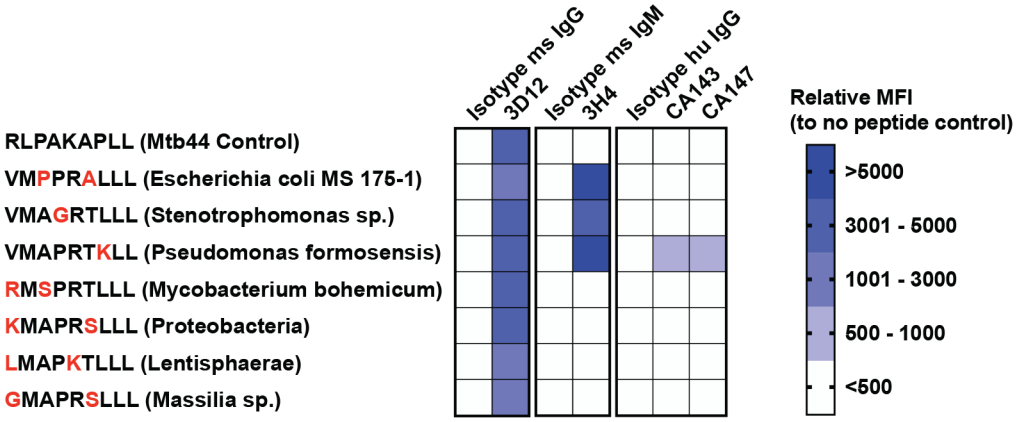

Figure 7. HLA-E-VL9-specific antibodies cross-react with certain microbiome-derived peptides presented by HLA-E. K562 cells loaded with microbiome-derived peptides were stained with the indicated antibodies at a concentration of 10 µg/ml. Binding activities are shown in heatmap form with relative MFIs (MFI of peptide-loaded cells minus MFI of no peptide control cells) depicted on the scale shown.